Electronic Supporting Information

Ruthenium(II) complexes with photoswitchable and photoejectable ligands

Kavisha A. Sarma, Isis A. Middleton, Man Him Chak, Jake P. Violi, Mohan Bhadbhade, William A. Donald, and Jonathon E. Beves.

Table of Contents

S1. Experimental

S1.1 General Experimental

Reagents and solvents were purchased from Sigma-Aldrich, Merck, Chem Supply or Combi-Blocks, and were used without purification unless stated otherwise. Anhydrous solvents were dispensed from an Inertcorp solvent purification system (model number: PS-MD-7). Automated column chromatography was performed on the Biotage® Selekt System using FlashPure EcoFlex Silica columns.

NMR spectroscopy was performed using a Bruker Avance III 400 with a Prodigy CryoProbe, a Bruker Avance III 500 with a TBI triple resonance room temperature probe and a Bruker Avance III 600 with a TCI helium CryoProbe. All chemical shifts were calibrated against residual solvent signals. All coupling constants (*J*) are reported in Hertz. Signals in the NMR spectra are reported as singlet (s), doublets (d), triplets (t), quartets (q), or unclear multiplets (m). NMR spectra were processed with MestReNova 14.1.2 software. All NMR data are assigned unambiguously, except where specified.

UV-vis experiments were performed on an Agilent Cary 60 Bio UV-visible Spectrophotometer equipped with a customized Cary Single Cell Peltier Accessory, keeping the samples at 25 °C unless stated otherwise. The cell holder was modified to allow for irradiation perpendicular to the direction of measurement. A Luxeon Rebel LED was mounted on a heat sink 4 cm from the cell and driven using a 1000 mA LuxDrive PowerPuck. The sample was analysed in a quartz cuvette with a path length of 1 cm. All samples were stirred to ensure homogeneity.

High-resolution mass spectrometry (HR-MS) experiments were performed on a hybrid linear quadrupole ion trap mass spectrometer (Thermo LTQ Orbitrap XL) equipped with an external nanospray ionisation (NSI) source in acetonitrile.

Table S1. Specifications for the LEDs used in this work.

LED part number (Supplier)	Dominant wavelength / nm
J035-L1C1GRN (Luxeon C Color LED)	530
J035-L1C1BLU (Luxeon C Color LED)	470
J035-L1C1VLT (Luxeon C Color LED)	425
BLS-LCS-0365-04-22 (Mightex BLS)	365

S1.2 Synthesis and characterisation of 1

S1.2.1 Synthesis of 1

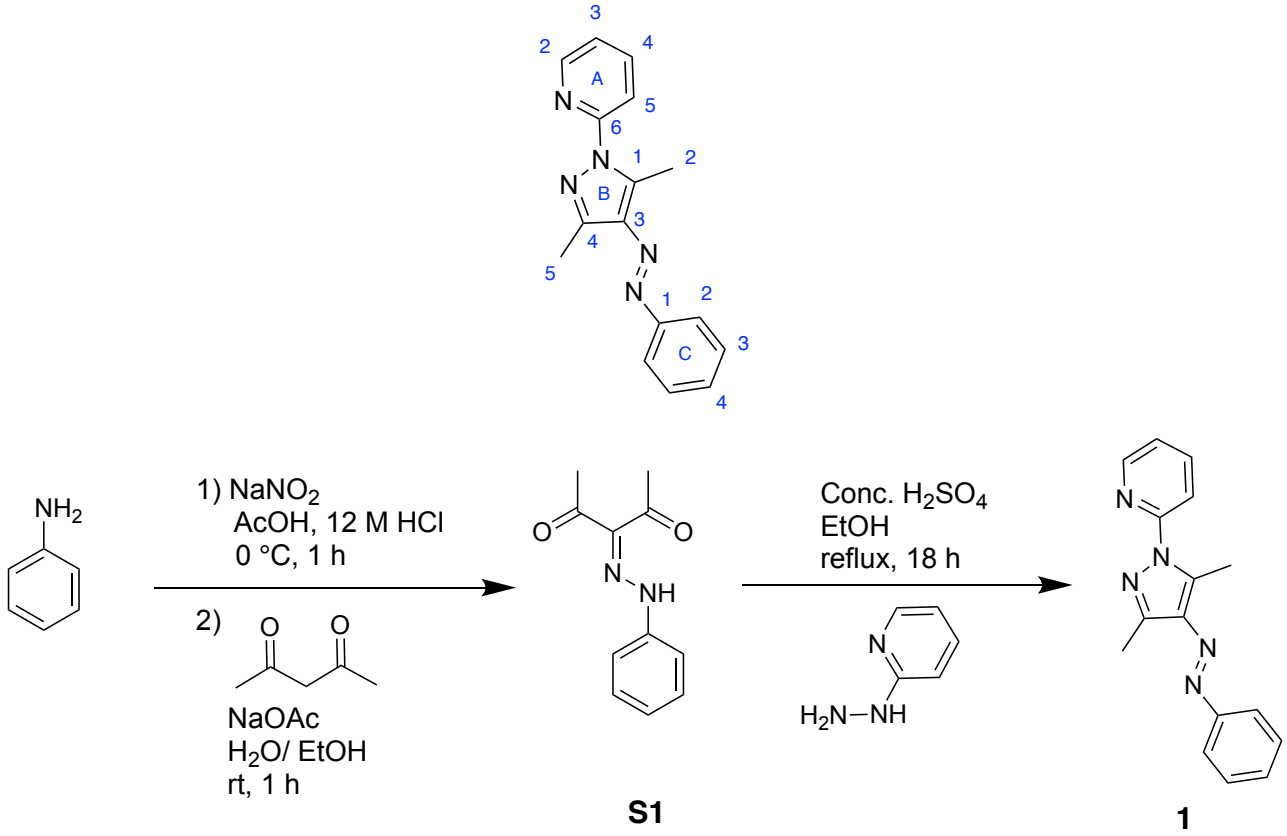

Intermediate 3-(2-phenylhydrazineylidene)pentane-2,4-dione (**S1**) was synthesised using a modification of literature procedures.[1] Ligand **1** has been previously synthesised using a different procedure.[2]

Sodium nitrite (620 mg, 9.0 mmol, 1.2 equiv.) in water (2.5 mL) was added dropwise to a solution of aniline (0.70 mL, 7.4 mmol, 1 equiv.) in HCl (32%, 1.7 mL) and acetone (10 mL) at 0 °C. The solution was stirred for an hour then transferred via syringe to a solution of acetyl acetone (0.98 mL, 9.6 mmol, 1.3 equiv.) and NaOAc (1.8 g, 22 mmol, 3 equiv.) in ethanol (7 mL) and water (4 mL). The solution was stirred at room temperature for an hour and the yellow precipitate was collected via vacuum filtration, washed with water (50 mL), 1:1 water:ethanol (50 mL) and hexane (50 mL to afford intermediate **S1** as a yellow solid (750 mg, 3.7 mmol, 50%) which was used without further purification.

Intermediate **S1** (700 mg, 3.4 mmol, 1 equiv.), 2-hydrazinopyridine (400 mg, 3.7 mmol, 1.1 equiv.) and sulfuric acid (0.60 mL, 98%) were dissolved in ethanol (50 mL). The solution was heated at reflux for 2 days and quenched with sodium bicarbonate until the pH reached 7. The solution was diluted into dichloromethane (100 mL) and the organic phase was washed with water (2 × 100 mL) and brine (2 × 100 mL). The organic layer was dried over Na_2SO_4 and the solvent was removed under reduced pressure. The residue was purified using column chromatography (silica, 0-2% MeOH/DCM and silica, 0-10% ethyl acetate/hexane) to afford ligand **1** as a yellow powder (700 mg, 2.5 mmol, 74%).

NMR data in $CDCl_3$ matches that reported.[2] Detailed NMR characterisation was conducted in CD_3CN for comparison with the later complexes.

^{1}H NMR (600 MHz, 298 K, acetonitrile-d_3) δ 8.50 (ddd, J = 4.9, 2.0, 1.0 Hz, 1H, H^{A2}), 7.95 (ddd, J = 8.4, 7.3, 2.0 Hz, 1H, H^{A4}) 7.89 (dt, J = 8.4, 1.0 Hz, 1H, H^{A5}), 7.84 (dd, J = 8.4, 1.3 Hz, 2H, H^{C2}), 7.53 (t, J = 7.6 Hz, 2H, H^{C3}), 7.46 (t, J = 7.6 Hz, 1H, H^{C4}), 7.34 (ddd, J = 7.3, 4.9, 1.0 Hz, 1H, H^{A3}), 2.99 (s, 3H, H^{B2}), 2.53 (s, 3H, H^{B5}).

^{13}C NMR (151 MHz, 298 K, acetonitrile-d_3) δ 154.4 (C^{C1}), 154.1 (C^{A6}), 148.8 (C^{A2}), 143.69 (C^{B4}),

143.66 (C^{B1}), 139.8 (C^{A4}), 137.7 (C^{B3}), 130.9 (C^{C4}), 130.1 (C^{C3}), 123.0 (C^{A3}), 122.7 (C^{C2}), 117.0 (C^{A5}), 15.1 (C^{B5}), 12.7 (C^{B2}).

UV-vis (298 K, acetonitrile): λ_{max} 337 nm ($\varepsilon = 4.7 \times 10^4$ M^{-1} cm^{-1}).

ESI-MS (m/z): 278.1395 $[M+H]^+$ (calc. 278.1406), 300.1218 $[M+Na]^+$ (calc. 300.1225).

S1.2.2 NMR characterisation of 1 in acetonitrile-d_3

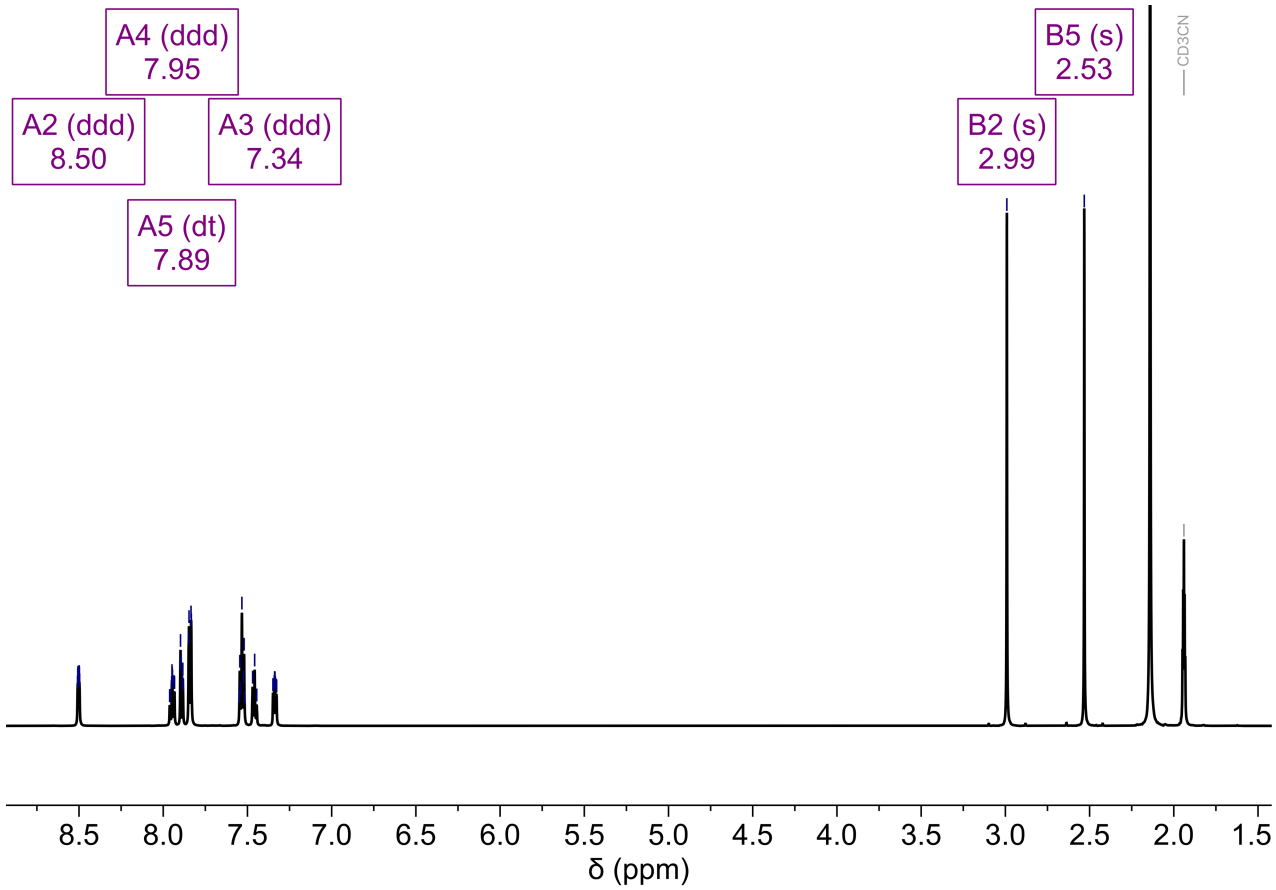

Figure S1. ^{1}H NMR (600 MHz, 298 K, acetonitrile-d_3) spectrum of **1**.

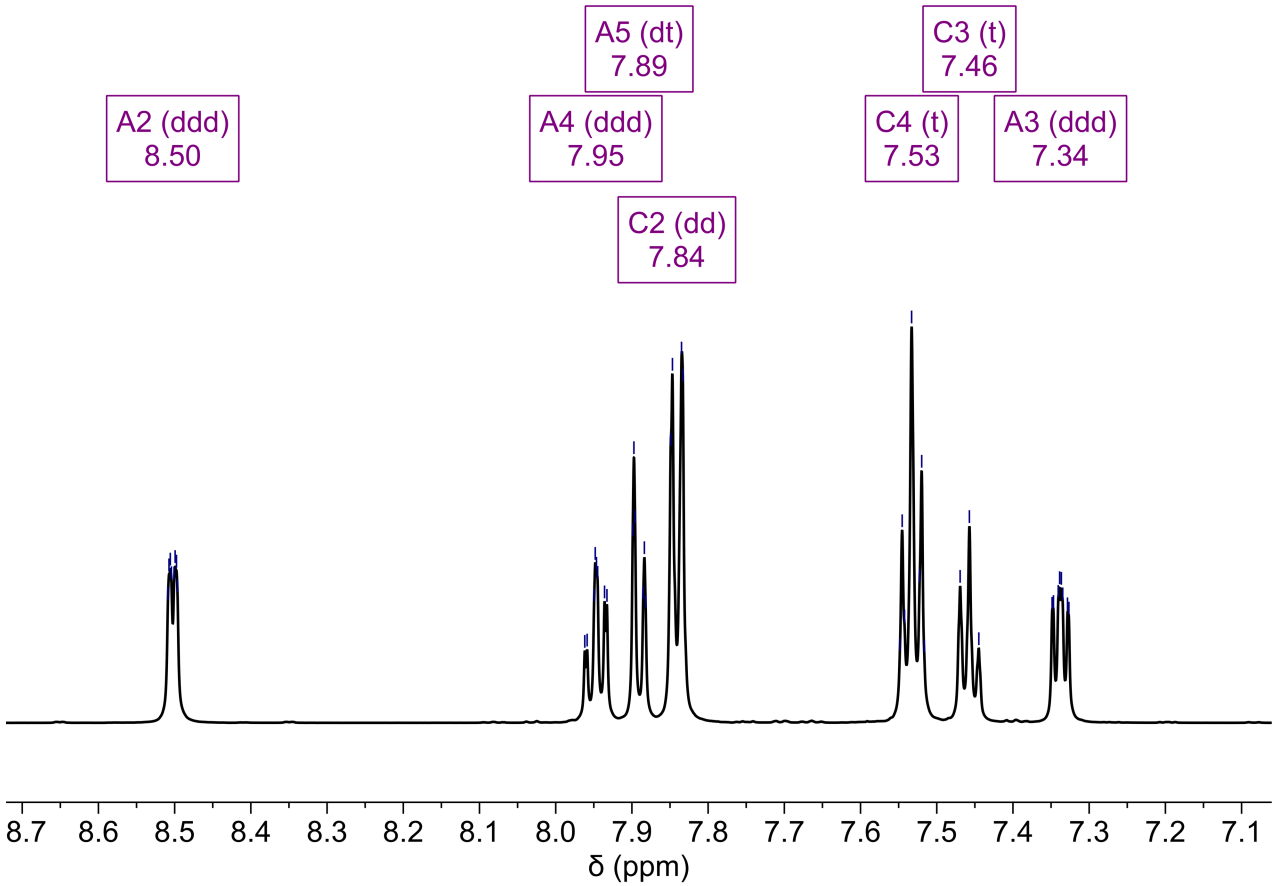

Figure S2. Partial ^{1}H NMR (600 MHz, 298 K, acetonitrile-d_3) spectrum of **1**.

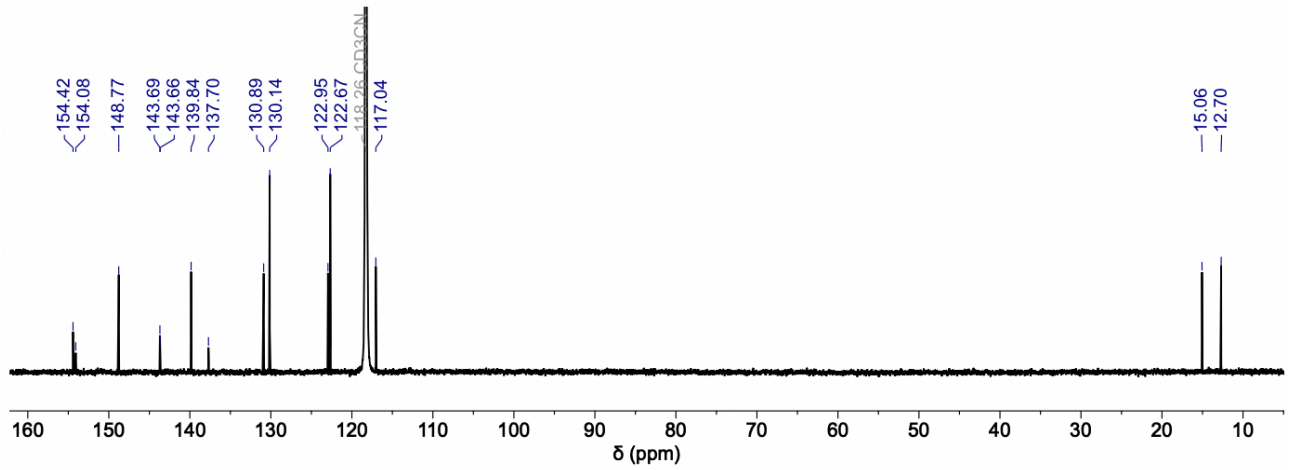

Figure S3. ^{13}C NMR (151 MHz, 298 K, acetonitrile-d_3) spectrum of **1**.

S1.3 Synthesis and characterisation of 2

S1.3.1 Synthesis of 2

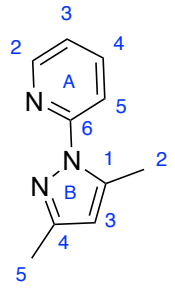

2-(3,5-Dimethyl-1*H*-pyrazol-1-yl)pyridine (**2**) was synthesised using a modification of literature procedures.[3]

Acetyl acetone (1.1 g, 10 mmol, 1 equiv.) 2-hydrazinopyridine (1.1 g, 10 mmol, 1 equiv.) and sulfuric acid (0.25 mL, 98%) were dissolved in ethanol (14 mL). The solution was heated at reflux for 21 h and quenched with sodium bicarbonate until the pH reached 7. The solution was diluted into dichloromethane (50 mL) and the organic phase was washed with water (2 × 50 mL) and brine (2 × 50 mL). The organic layer was dried over Na_2SO_4, and the solvent was removed under reduced pressure. The residue was purified using column chromatography (silica, 0-10% ethyl acetate/hexane) to afford the product as a clear liquid (700 mg, 0.4 mmol, 40%).

NMR data in $CDCl_3$ matches that reported.[3] Detailed NMR characterisation was conducted in CD_3CN for comparison with the later complexes.

^{1}H NMR (600 MHz, 298 K, acetonitrile-d_3) δ 8.40 (ddd, J = 4.9, 2.0, 1.0 Hz, 1H, H^{A2}), 7.86 (ddd, J = 8.4, 7.3, 2.0 Hz, 1H, H^{A4}), 7.80 (dt, J = 8.4, 1.0 Hz, 1H, H^{A5}), 7.22 (ddd, J = 7.3, 4.9, 1.0 Hz, 1H, H^{A3}), 6.04 (s, 1H, H^{B3}), 2.60 (s, 3H, H^{B2}), 2.22 (s, 3H, H^{B5}).

^{13}C NMR (151 MHz, 298 K, acetonitrile-d_3) δ 154.6 (C^{A6}) 150.4 (C^{B4}), 148.4 (C^{A2}), 142.3 (C^{B1}), 139.5 (C^{A4}), 121.8 (C^{A3}), 116.4 (C^{A2}), 109.7 (C^{B3}), 14.6 (C^{B2}), 13.6 (C^{B5}).

UV-vis (298 K, acetonitrile): λ_{max} 255 nm (ε = 1.1 × 10^4 M^{-1} cm^{-1}).

ESI-MS (m/z): 174.1022 $[M+H]^+$ (calculated: 174.1031), 196.0841 $[M+Na]^+$ (calculated: 196.0851).

S1.3.1 NMR characterisation of 2 in acetontrile-d_3

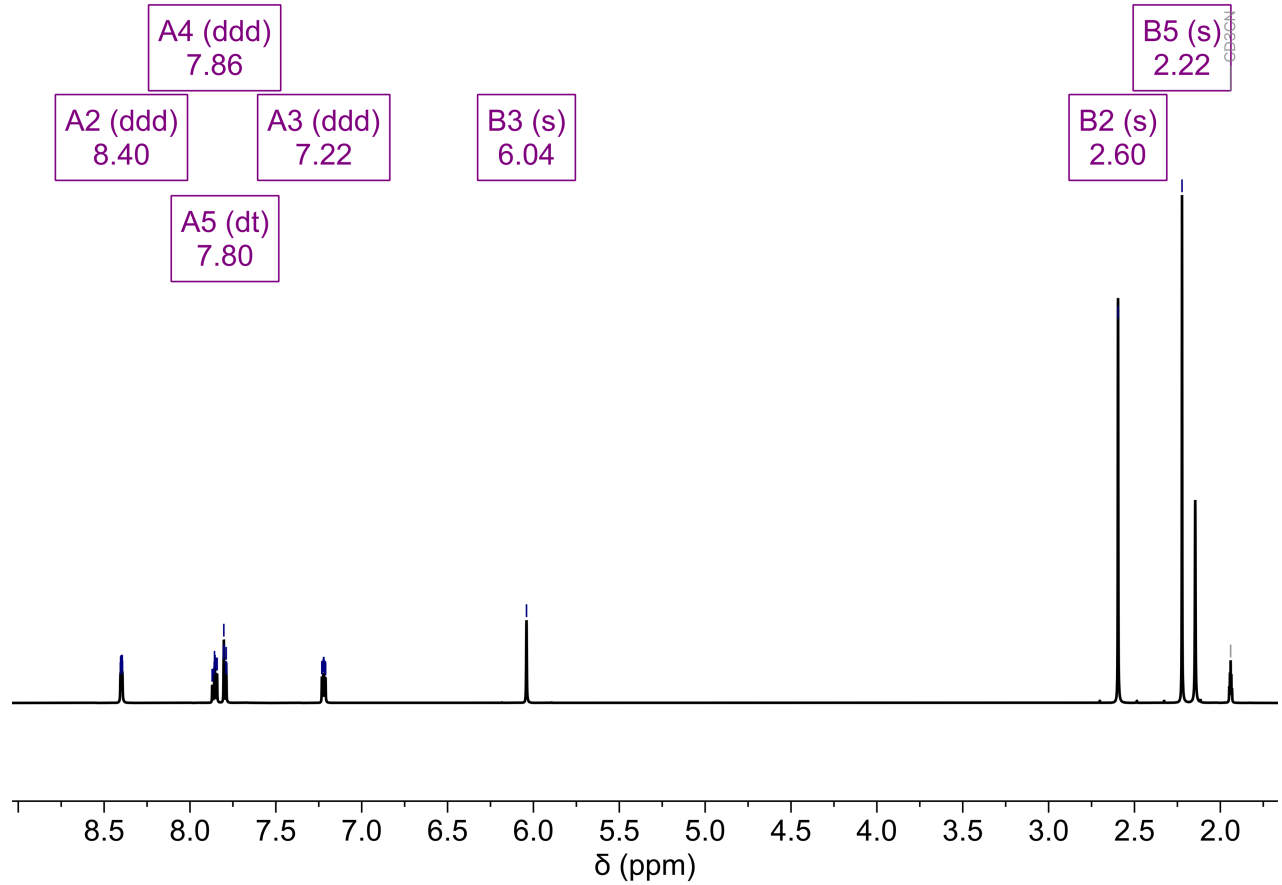

Figure S4. ^{1}H NMR (600 MHz, 298 K, acetonitrile-d_3) spectrum of **2**.

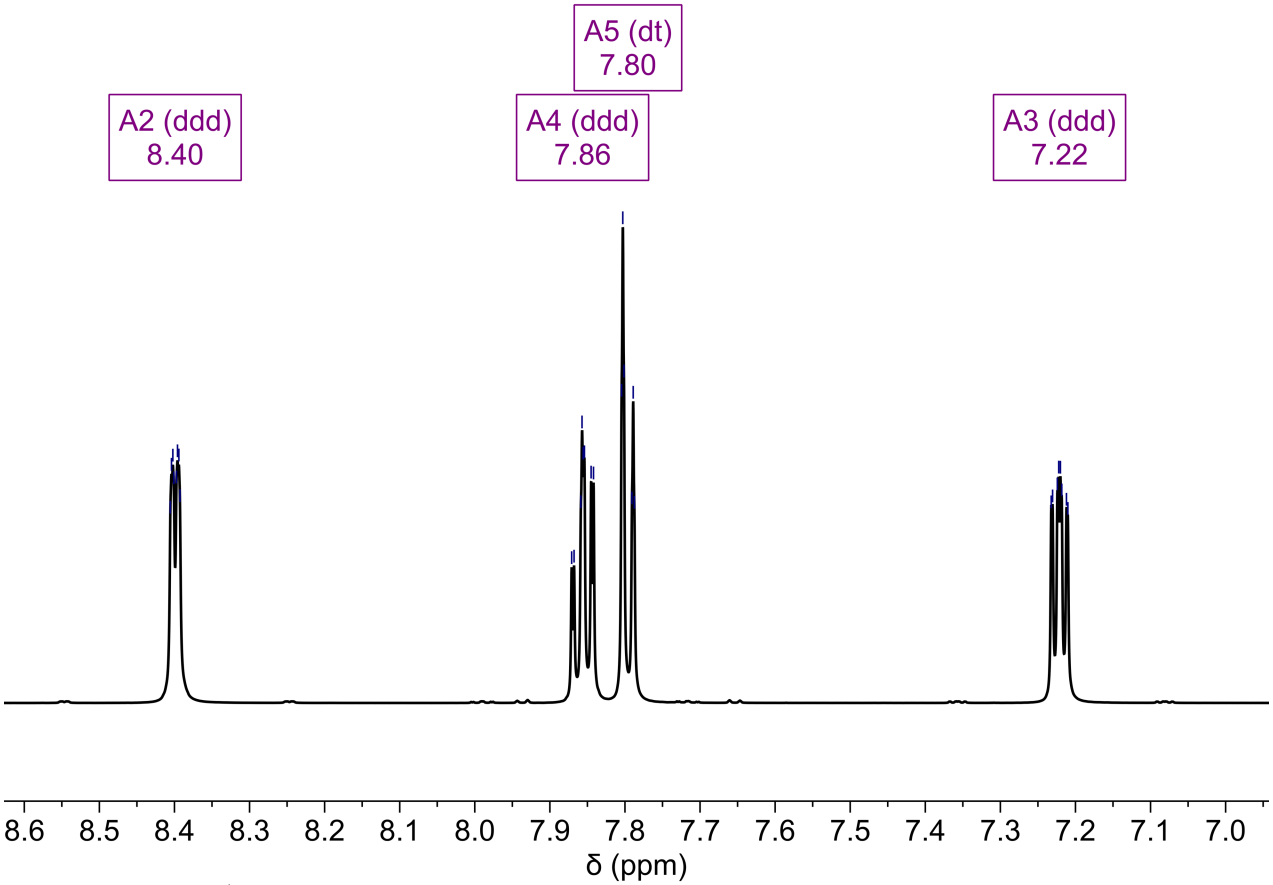

Figure S5. Partial ^{1}H NMR (600 MHz, 298 K, acetonitrile-d_3) spectrum of **1**.

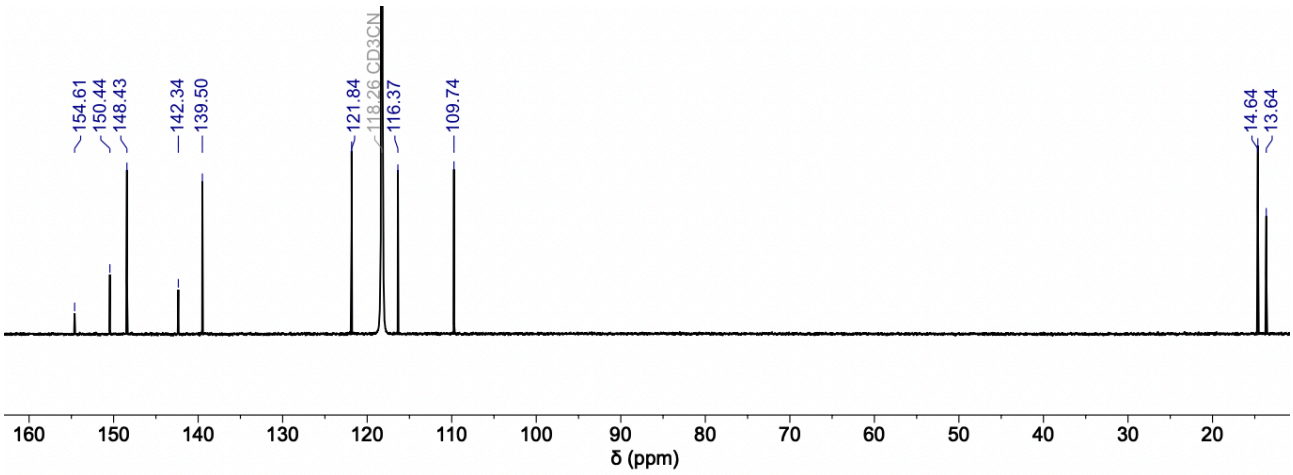

Figure S6. ^{13}C NMR (151 MHz, 298 K, acetonitrile-d_3) spectrum of **2**.

S1.4 Synthesis of $Ru(bpy)_2Cl_2$

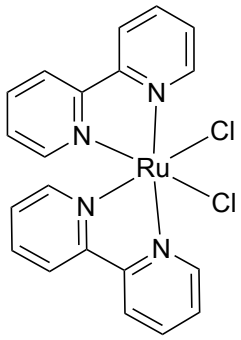

$Ru(bpy)_2Cl_2$ was synthesised using modified literature procedures.[4, 5]

$RuCl_3 \cdot 3H_2O$ (790 mg, 3.0 mmol, 1 equiv.), 2,2'-bipyridine (950 mg, 6.0 mmol, 2 equiv.) and LiCl (840 mg, 20 mmol, 7 equiv.) were suspended in *N*,*N*-dimethylformamide (13 mL). The solution was heated at reflux for 8 h and diluted with acetone (100 mL), then cooled at 0 °C for 16 hours then filtered through filter paper. The solid was washed with water (3 × 25 mL) and ethanol (3 × 25 mL) and dried by suction to afford the product as a black solid (890 mg, 1.8 mmol, 61%) which was used without further purification.

S1.5 Synthesis and characterisation of [Ru(bpy)$_2$(*E*-1)](PF$_6$)$_2$

S1.5.1 Synthesis of [Ru(bpy)$_2$(*E*-1)](PF$_6$)$_2$

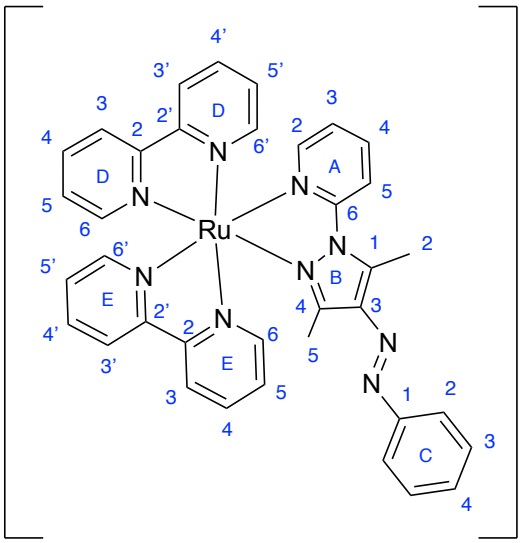

Complex [Ru(bpy)$_2$(*E*-**1**)](PF$_6$)$_2$ was prepared using an adaptation of literature methods for related complexes.[4]

Ru(bpy)$_2$Cl$_2$ (100 mg, 0.2 mmol, 1 equiv.) and **1** (550 mg, 0.26 mmol, 1.2 equiv.) were suspended in ethylene glycol (6 mL) in a 10 mL microwave sample vial. The reaction mixture was heated at 160 °C for 15 minutes in a microwave reactor. The reaction mixture was poured into aqueous KPF_6 (1.5 g in 100 mL of water). The precipitate was collected on Celite and washed with water (3 × 50 mL). The residue was dissolved in acetonitrile which was removed under reduced pressure, and the residue was purified using column chromatography (silica, 40:4:1 acetonitrile/$KNO_{3(aq)}$/water). The main red band was concentrated under reduced pressure and poured into saturated aqueous KPF_6 (30 mL). The precipitate was collected on Celite and washed with water (3 × 50 mL). The residue was dissolved in acetonitrile which was removed under reduced pressure to afford the product as an orange solid (48 mg, 0.05 mmol, 23%). Due to many very close signals in both the ^{1}H and ^{13}C NMR spectra it was not possible to unambiguously assign all signals.

^{1}H NMR (600 MHz, 298 K, acetonitrile-d_3) δ 8.55 – 8.44 (m, 4H, H^{D6}, $H^{D6'}$, H^{E6}, $H^{E6'}$), 8.23 (d, 1H, H^{A5}), 8.18 (ddd, *J* = 5.6, 1.5, 0.8 Hz, 1H, H^{E3}), 8.15 – 7.98 (m, 5H, H^{A4}, H^{D5}, $H^{D5'}$, H^{E5}, $H^{E5'}$), 7.88 – 7.81 (m, 3H, H^{C3}, $H^{D3'}$), 7.77 (ddd, *J* = 5.7, 1.5, 0.7 Hz, 1H, H^{D3}), 7.62 (ddd, *J* = 5.6, 1.5, 0.7 Hz, 1H, $H^{E3'}$), 7.58 (ddd, *J* = 5.8, 1.7, 0.7 Hz, 1H, H^{A2}), 7.56 – 7.44 (m, 5H, H^{C2}, H^{C3}, $H^{D4'}$, H^{E4}), 7.41 – 7.32 (m, 2H, H^{D5}, $H^{E4'}$), 7.26 (ddd, *J* = 7.5, 5.7, 1.1 Hz, 1H, H^{A3}), 3.23 (s, 1H, H^{B2}), 1.87 (s, 1H, H^{B5}).

^{13}C NMR (151 MHz, 298 K, acetonitrile-d_3) δ 157.8, 153.6 (H^{E3}), 153.0, 152.9, 152.7 (H^{D3}), 152.5 ($H^{E3'}$), 152.0 (H^{A2}), 151.2, 146.2, 140.8, 139.1, 139.0, 138.9, 138.8, 132.5, 130.4, 128.8, 128.6, 128.4, 128.5, 125.4, 125.4, 125.4, 125.3, 124.9 (H^{A3}), 123.2, 115.6 (H^{A5}), 66.3, 61.0,15.6, 14.5, 13.5 (H^{B2}), 12.8 (H^{B5}).

UV-vis (298 K, acetonitrile): λ_{max} 287 nm (ε = 7.7 × 10^4 M^{-1} cm^{-1}), MLCT λ_{max} 411 nm (ε = 1.5 × 10^4 M^{-1} cm^{-1}).

S1.5.2 NMR characterisation of [Ru(bpy)$_2$(*E*-1)](PF$_6$)$_2$ in acetonitrile-d_3

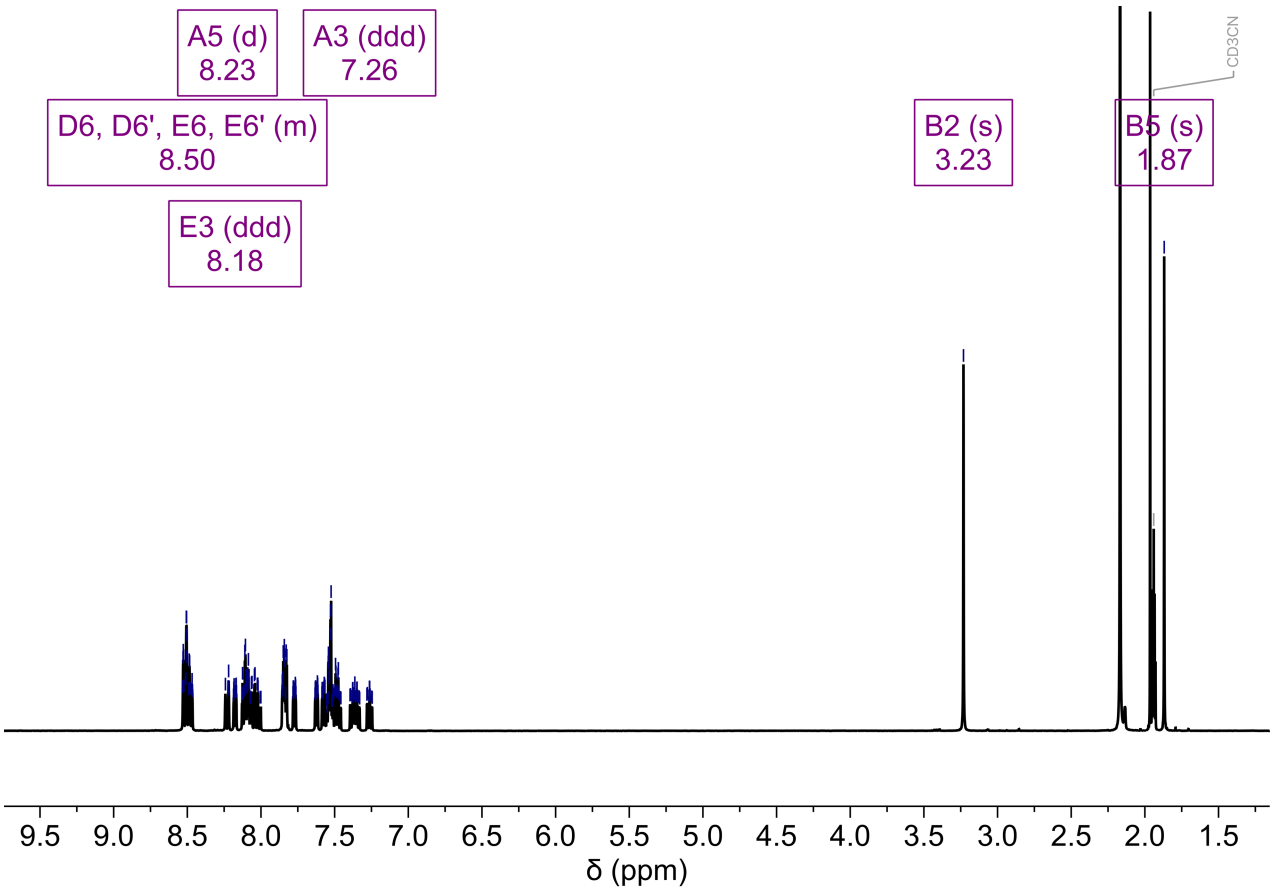

Figure S7. ^{1}H NMR (600 MHz, 298 K, acetonitrile-d_3) spectrum of [Ru(bpy)$_2$(*E*-**1**)](PF$_6$)$_2$.

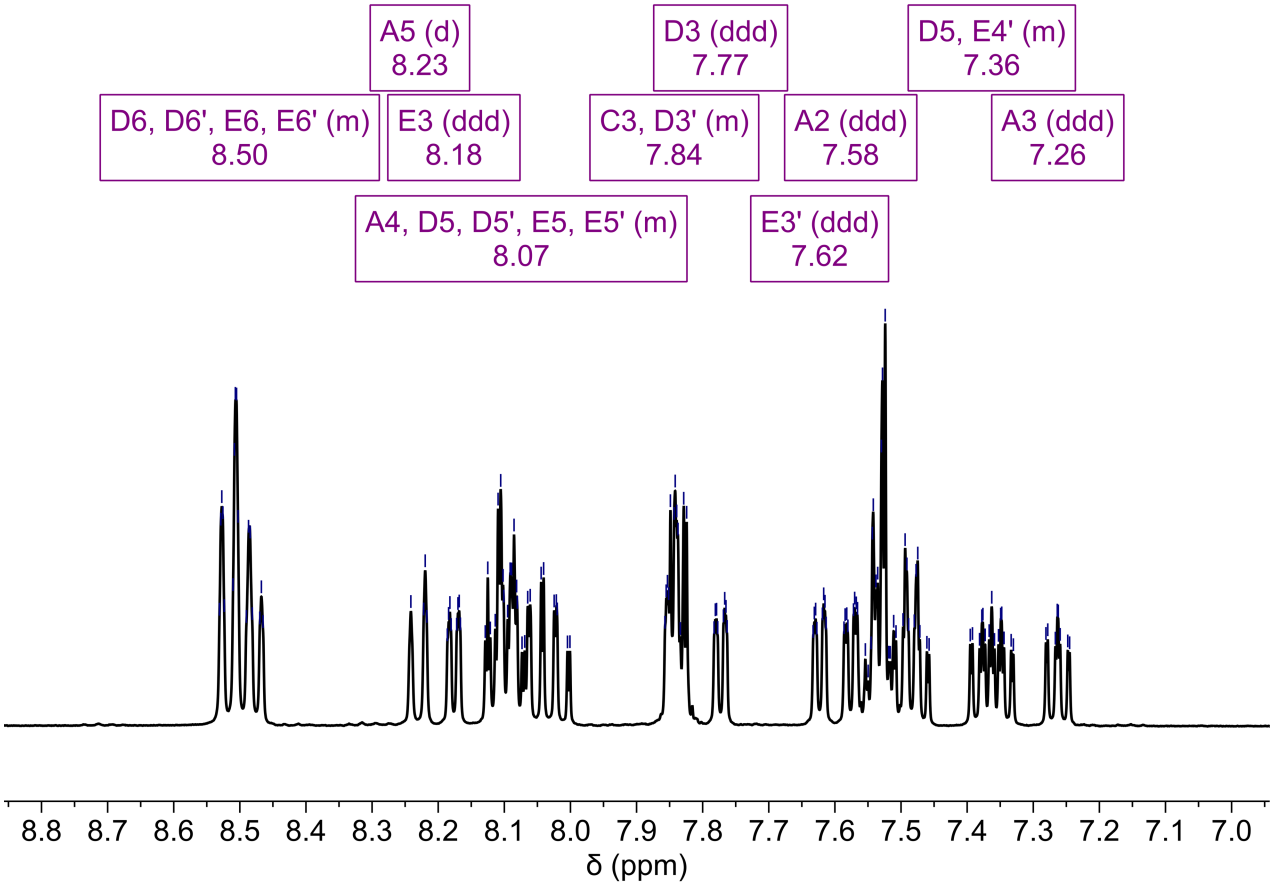

Figure S8. Partial ^{1}H NMR (600 MHz, 298 K, acetonitrile-d_3) spectrum of [Ru(bpy)$_2$(*E*-**1**)](PF$_6$)$_2$.

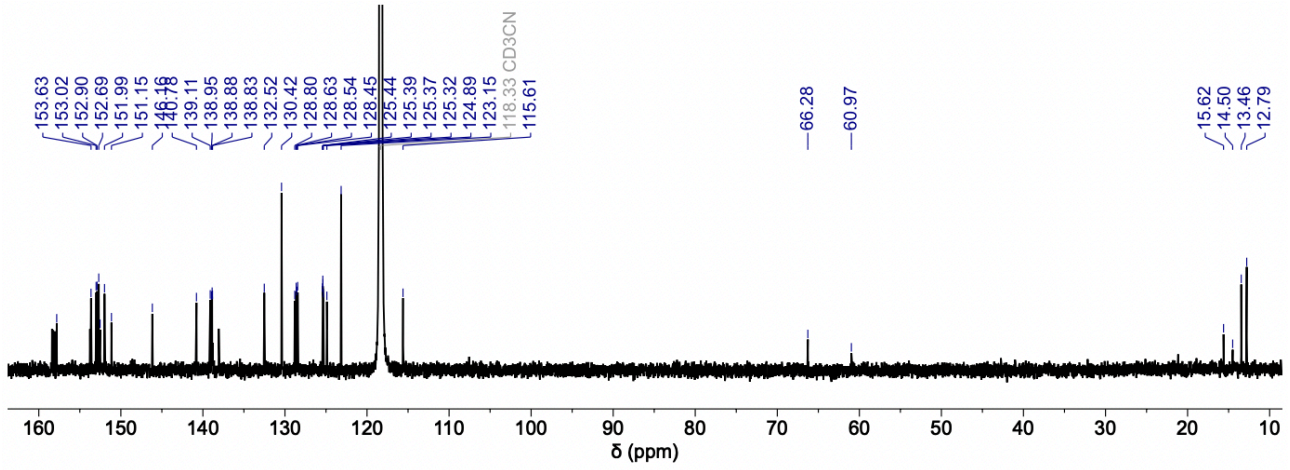

Figure S9. ^{13}C NMR (151 MHz, 298 K, acetonitrile-d_3) spectrum of [Ru(bpy)$_2$(*E*-**1**)](PF$_6$)$_2$.

S1.5.3 ESI-MS of [Ru(bpy)$_2$(*E*-1)](PF$_6$)$_2$ in acetonitrile

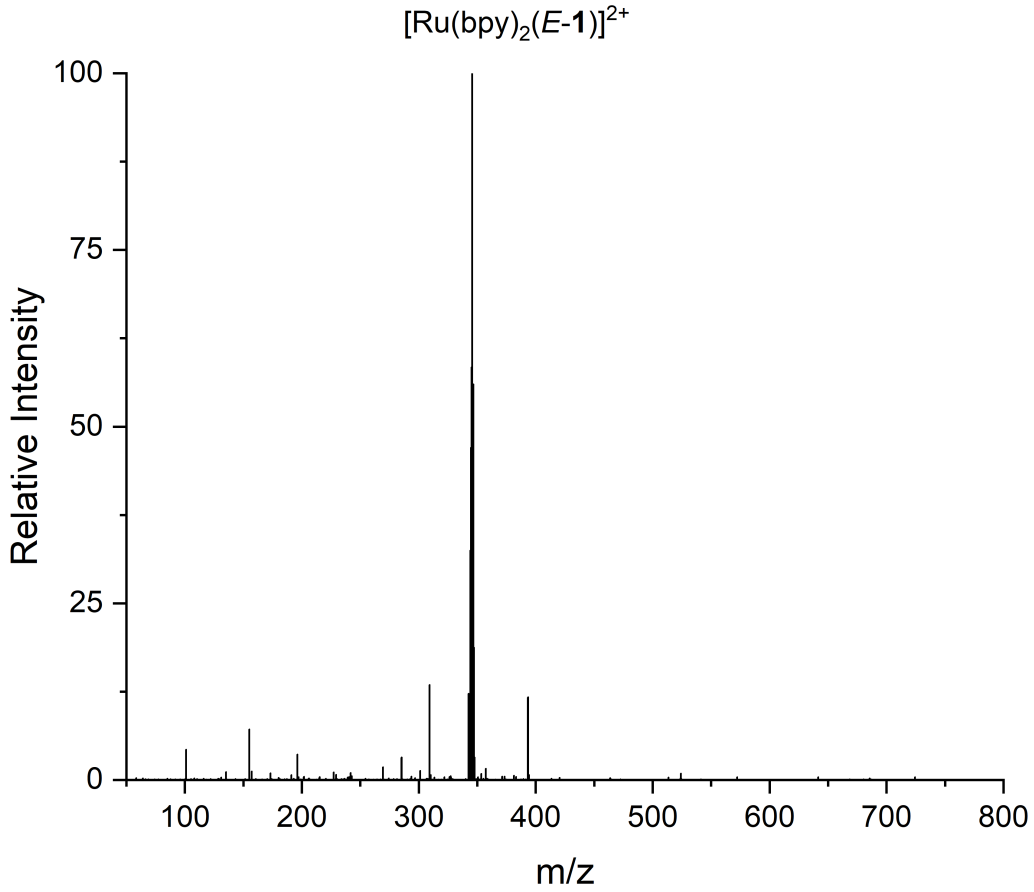

Figure S10. ESI-MS of [Ru(bpy)$_2$(*E*-**1**)](PF$_6$)$_2$ in acetonitrile.

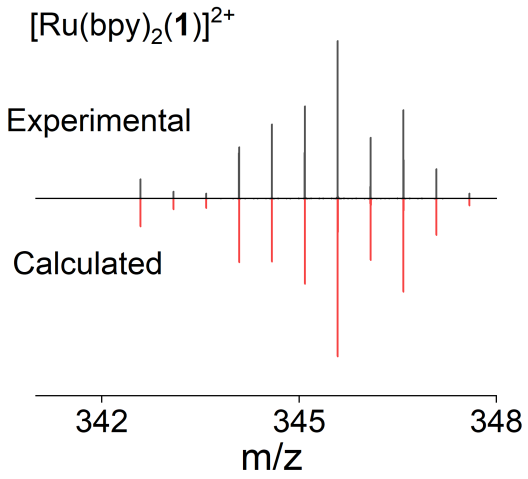

Figure S11 Zoom scan of select ESI-MS peak, with simulated isotope pattern of $[Ru(bpy)_2(E\text{-}\mathbf{1})](PF_6)_2$.

S1.6 Synthesis and characterisation of $[Ru(bpy)_2(2)](PF_6)_2$

S1.6.1 Synthesis of $[Ru(bpy)_2(2)](PF_6)_2$

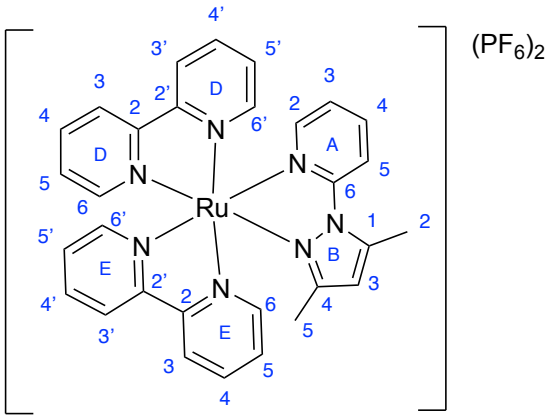

Complex $[Ru(bpy)_2(\mathbf{2})](PF_6)_2$ was prepared using an adaptation of literature methods for related complexes.[4] The product obtained matches literature NMR data,[6, 7] and detailed characterisation was performed.

$Ru(bpy)_2Cl_2$ (100 mg, 0.22 mmol, 1 equiv.) and 2-(3,5-dimethyl-1*H*-pyrazol-1-yl)pyridine (**2**) (46 mg, 0.26 mmol, 1.2 equiv.) were suspended in ethylene glycol (6 mL) in a 10 mL microwave sample vial. The reaction mixture was heated at 160 °C for 15 minutes in a microwave reactor. The reaction mixture was poured into aqueous KPF_6 (1.6 g in 100 mL water). The precipitate was collected on Celite and washed with water (3 × 50 mL). The solid was dissolved in acetonitrile which was removed under reduced pressure. The residue was purified using column chromatography (silica, 10:1:1 acetonitrile/$KNO_{3(aq)}$/water). The main red band was collected and concentrated under reduced pressure, then poured into saturated aqueous KPF_6 (30 mL). The precipitate was collected on Celite washed with water (3 × 50 mL), dissolved in acetonitrile and the solvent removed under reduced pressure to afford the product as a pink solid (180 mg, 0.20 mmol, 93%). Due to many very close signals in both the ^1H and ^{13}C NMR spectra it was not possible to unambiguously assign all signals.

^1H NMR (600 MHz, 298 K, acetonitrile-d_3) δ 8.53 – 8.43 (m, 4H, H^{D6}, $H^{D6'}$, H^{E6}, $H^{E6'}$), 8.12 – 7.95 (m, 7H, H^{A4}, H^{A5}, H^{D5}, $H^{D5'}$, H^{E3}, H^{E5}, $H^{E5'}$), 7.80 (ddd, *J* = 5.6, 1.5, 0.8 Hz, 1H, $H^{D3'}$), 7.75 (ddd, *J* = 5.7, 1.5, 0.8 Hz, 1H, H^{D3}), 7.61 (ddd, *J* = 5.6, 1.5, 0.8 Hz, 1H, $H^{E3'}$), 7.52 (ddd, *J* = 5.8, 1.7, 0.8 Hz, 1H, H^{A2}), 7.48 (ddd, *J* = 7.7, 5.6, 1.3 Hz, 1H, H^{E4}), 7.45 (ddd, *J* = 7.7, 5.6, 1.5 Hz, 1H, $H^{D4'}$), 7.35 (ddd, *J* = 7.6, 5.6, 1.5 Hz, 1H, $H^{E4'}$), 7.32 (ddd, *J* = 7.3, 5.7 1.5 Hz, 1H, H^{D4}), 7.18 (ddd, *J* = 6.9, 5.8, 1.7 Hz, 1H, H^{A3}), 6.35 (s, 1H, H^{B3}), 2.83 (s, 2H, H^{B2}), 1.49 (s, 3H, H^{B5}).

^{13}C NMR (151 MHz, 298 K, acetonitrile-d_3) δ 158.4, 158.3, 158.1, 157.8, 157.3, 153.2, 153.0 (H^{D3}), 152.8, 152.7 ($H^{D3'}$), 152.6 ($H^{E3'}$), 151.6 (H^{A2}), 146.6, 140.5, 138.8, 138.7, 138.6, 138.5, 128.64 ($H^{E4'}$), 128.56 (H^{E4}), 128.4 ($H^{D4'}$), 128.3 (H^{D4}), 125.3, 125.2, 125.2, 125.1, 124.1 (H^{A3}), 114.6 (H^{B3}), 114.5, 15.6 (H^{B2}), 12.5 (H^{B5}).

UV-vis (298 K, acetonitrile): λ_{max} 285 nm (ε = 5.7 × 10^4 M^{-1} cm^{-1}). MLCT λ_{max} 449 nm (ε = 8.1 × 10^3 M^{-1} cm^{-1}).

S1.6.2 NMR characterisation of $[Ru(bpy)_2(2)](PF_6)_2$ in acetonitrile-d_3

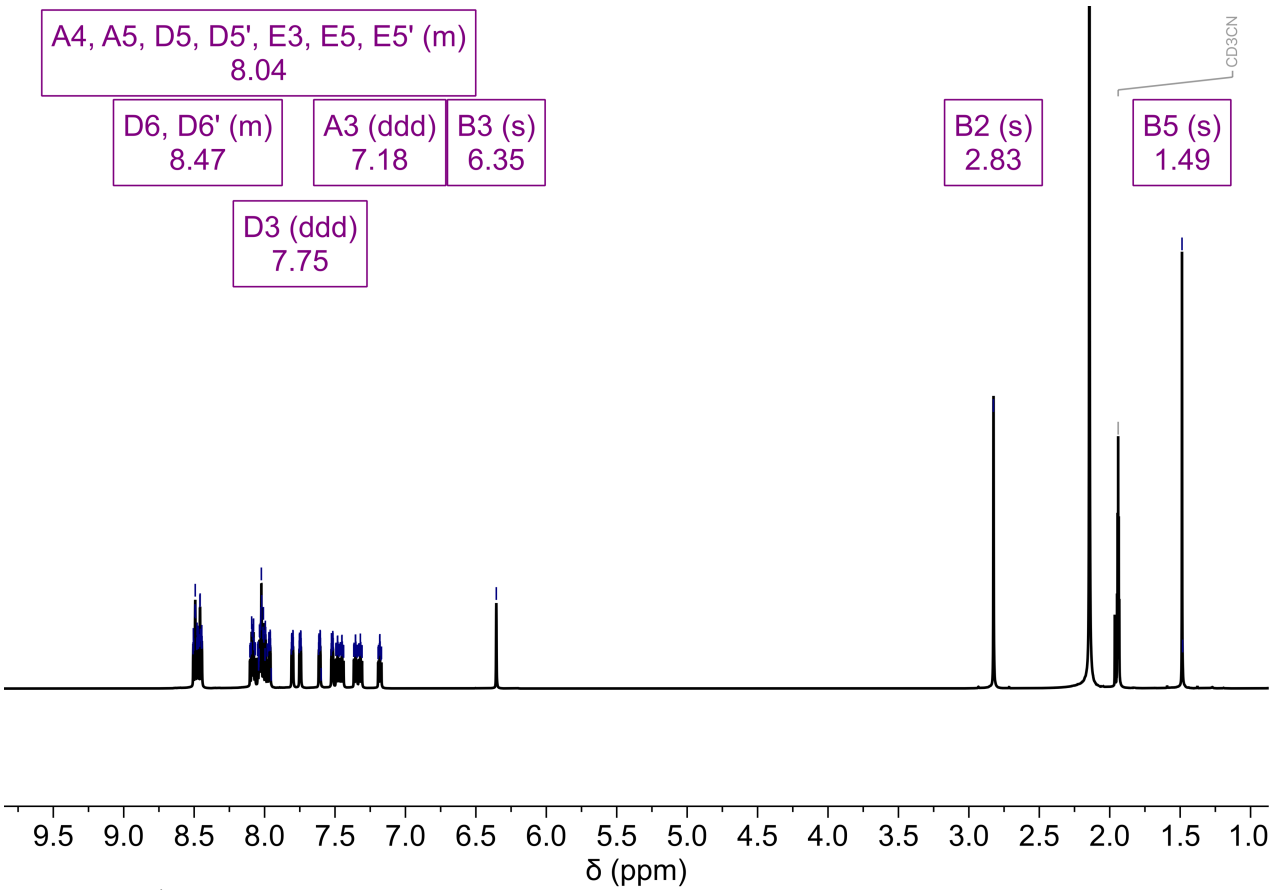

Figure S12. ^{1}H NMR (600 MHz, 298 K, acetonitrile-d_3) spectrum of $[Ru(bpy)_2(\mathbf{2})](PF_6)_2$.

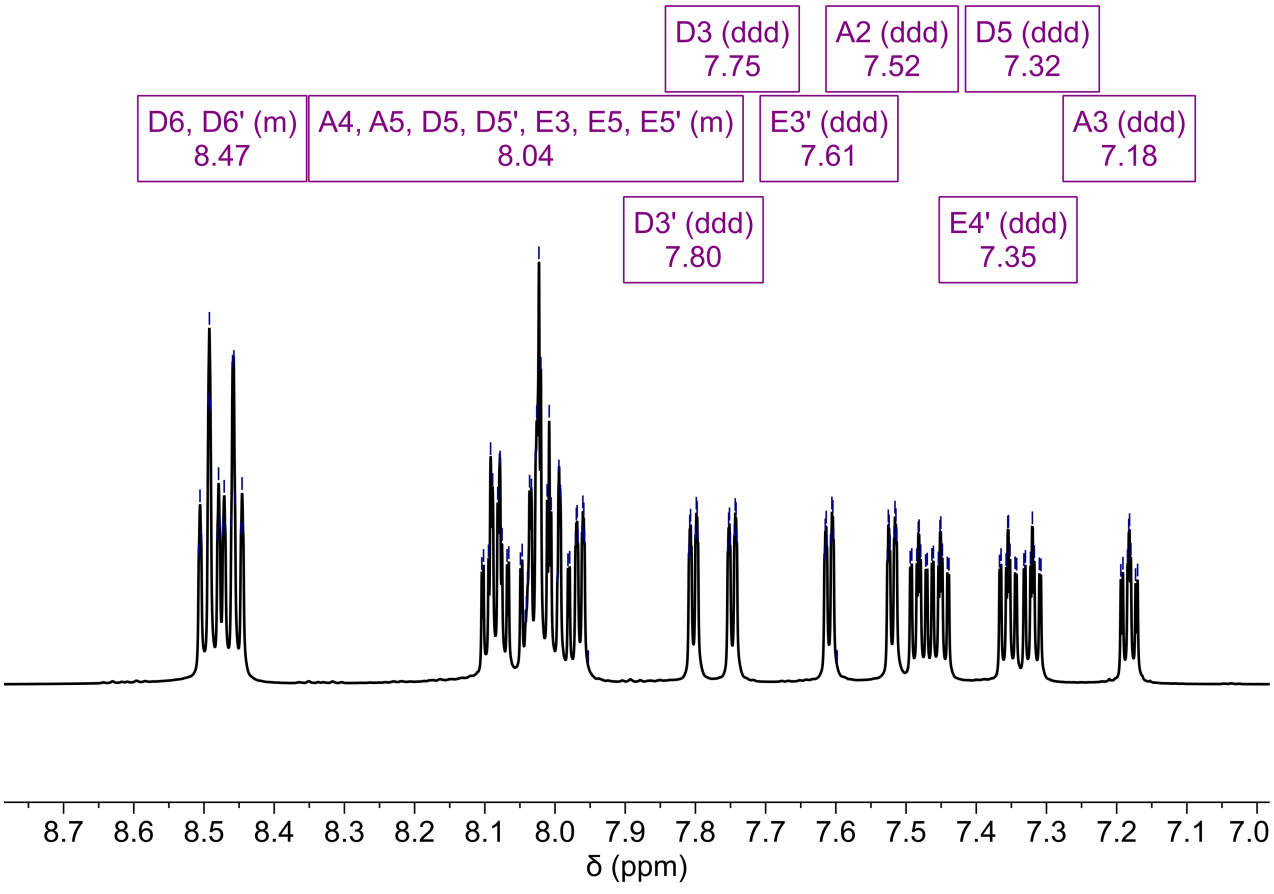

Figure S13. Partial ^{1}H NMR (600 MHz, 298 K, acetonitrile-d_3) spectrum of $[Ru(bpy)_2(\mathbf{2})](PF_6)_2$.

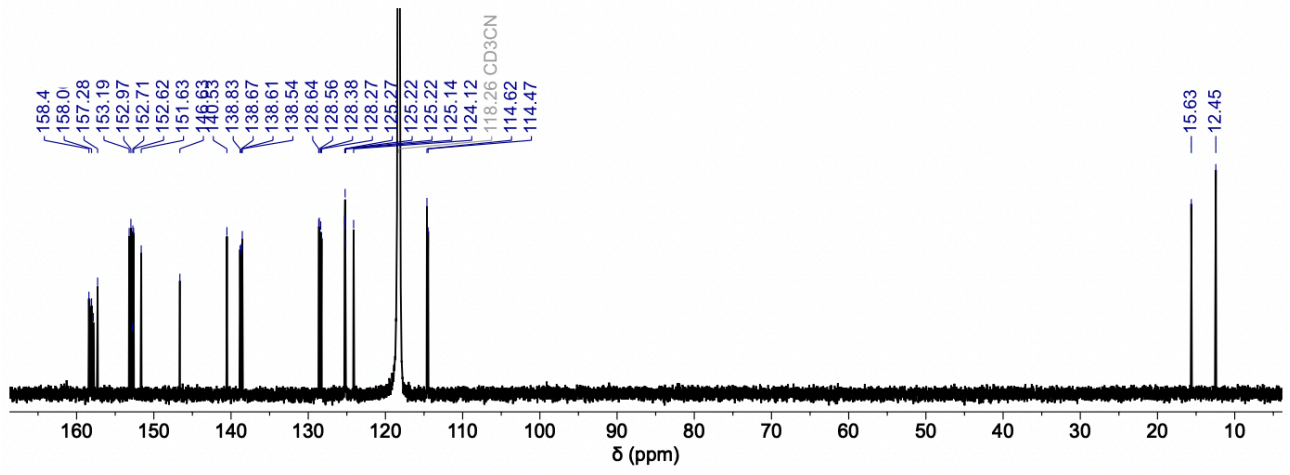

Figure S14. ^{13}C NMR (151 MHz, 298 K, acetonitrile-d_3) spectrum of $[Ru(bpy)_2(\mathbf{2})](PF_6)_2$.

S1.6.3 ESI-MS of $[Ru(bpy)_2(2)](PF_6)_2$ in acetonitrile

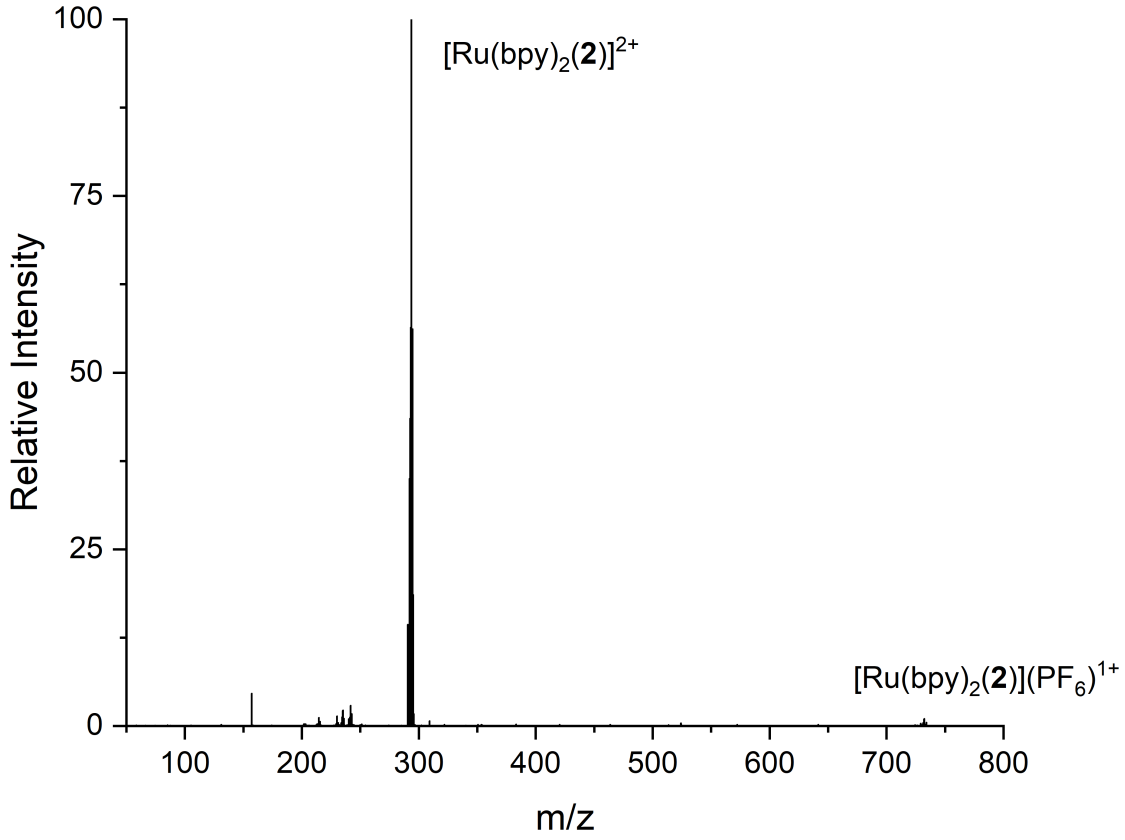

Figure S15. ESI-MS spectrum of $[Ru(bpy)_2(\mathbf{2})](PF_6)_2$ in acetonitrile.

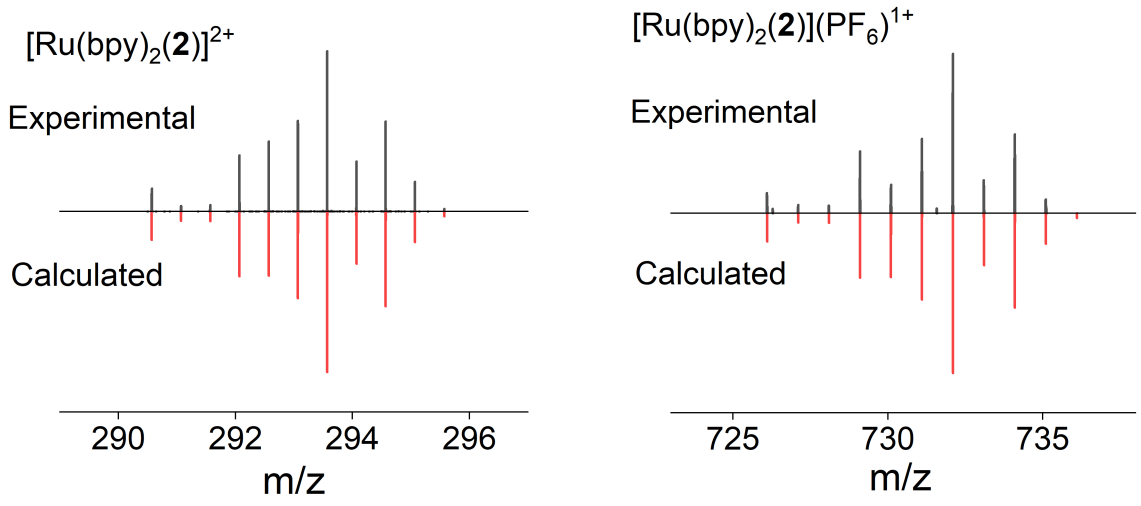

Figure S16. Zoom scans of select ESI-MS peaks, with simulated isotope patterns of $[Ru(bpy)_2(\mathbf{2})](PF_6)_2$.

S1.7 Synthesis and characterisation of $[Ru(bpy)_2(MeCN)_2](PF_6)_2$

S1.7.1 Synthesis of $[Ru(bpy)_2(MeCN)_2](PF_6)_2$

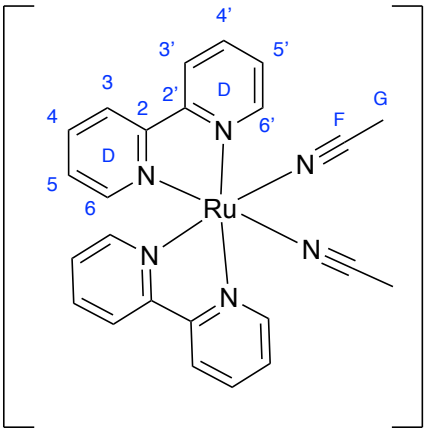

$Ru(MeCN)_2(bpy)_2](PF_6)_2$ was synthesised using a modification of literature procedures and the product obtained matches literature NMR characterisation.[8, 9]

$Ru(bpy)_2Cl_2$ (250 mg, 0.52 mmol, 1 equiv.) was added to a solution of acetonitrile (2 mL) and H_2O (2 mL). Argon was bubbled through to degas the solution which was heated at 75 C for 1 h while covered in foil. The solution cooled to room temperature and was poured into saturated aqueous KPF_6 (5 mL) to form a precipitate which was collected on Celite and dissolved in DCM which was removed under reduced pressure to afford the product as an orange solid (190 mg, 0.24 mmol, 46%).

^{1}H NMR (600 MHz, 298 K, acetonitrile-d_3) δ 9.30 (ddd, J = 5.5, 1.5, 0.8 Hz, 1H, H^{D6}), 8.50 (d, J = 8.1 Hz, 1H, H^{D3}), 8.36 (d, J = 8.1 Hz, 1H, $H^{D3'}$), 8.26 (td, J = 7.9, 1.5 Hz, 1H, H^{D4}), 7.94 (td, J = 7.9, 1.5 Hz, 1H, $H^{D4'}$), 7.84 (ddd, J = 7.9, 5.5, 1.5 Hz, 1H, H^{D5}), 7.58 (dd, J = 5.5, 0.8 Hz, 1H $H^{D6'}$), 7.25 (ddd, J = 7.8, 5.5, 1.5 Hz, 1H, $H^{D5'}$), 2.26 (s, 3H, H^{G}).

^{13}C NMR (151 MHz, 298 K, acetonitrile-d_3) δ 158.9 ($H^{D2'}$), 158.1 (H^{D2}), 154.2 (H^{D6}), 153.1 ($H^{D6'}$), 139.3 (H^{D4}), 138.9 ($H^{D4'}$), 128.4 (H^{D5}), 127.7 (H^{D5}), 126.7 (H^{F}), 124.8 (H^{D3}), 124.5 ($H^{D3'}$), 4.5 (H^{G}).

UV-vis (298 K, acetonitrile): λ_{max} 284 nm (ε = 4.3 × 10^4 M^{-1} cm^{-1}). MLCT λ_{max} 426 nm (ε = 6.5 × 10^3 M^{-1} cm^{-1}).

S1.7.2 NMR characterisation of $[Ru(bpy)_2(MeCN)_2](PF_6)_2$ in acetonitrile-d_3

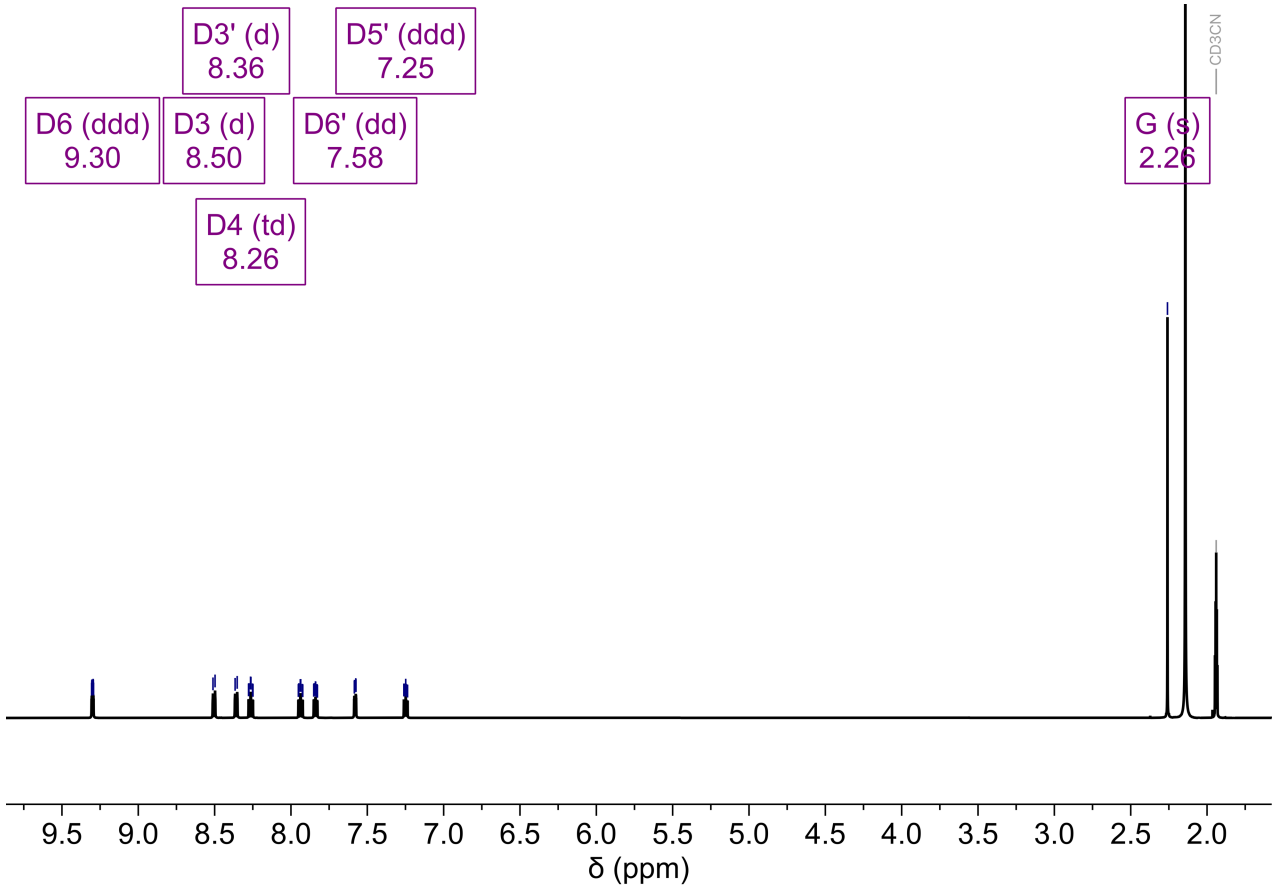

Figure S17. ^{1}H NMR (600 MHz, 298 K, acetonitrile-d_3) spectrum of $[Ru(bpy)_2(MeCN)_2](PF_6)_2$.

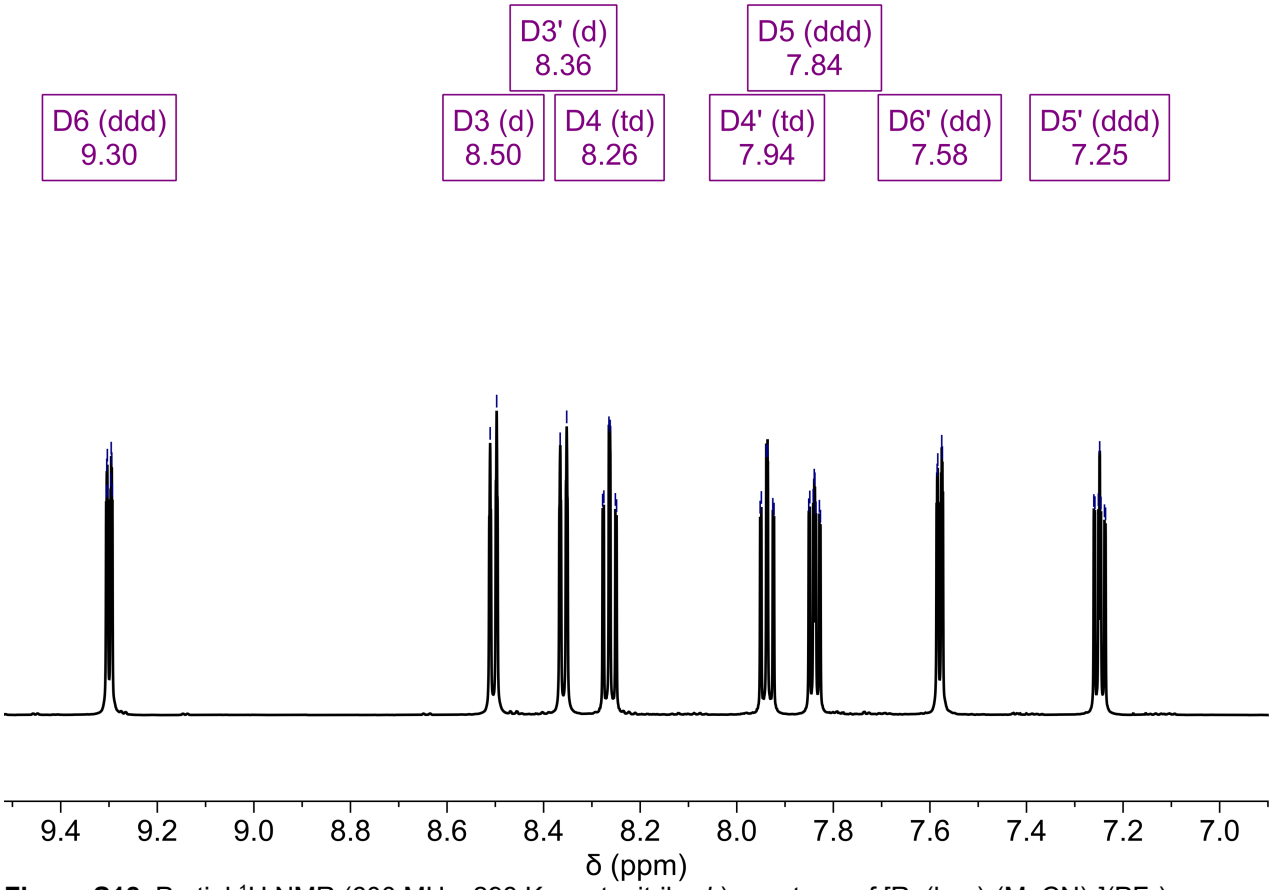

Figure S18. Partial ^{1}H NMR (600 MHz, 298 K, acetonitrile-d_3) spectrum of $[Ru(bpy)_2(MeCN)_2](PF_6)_2$.

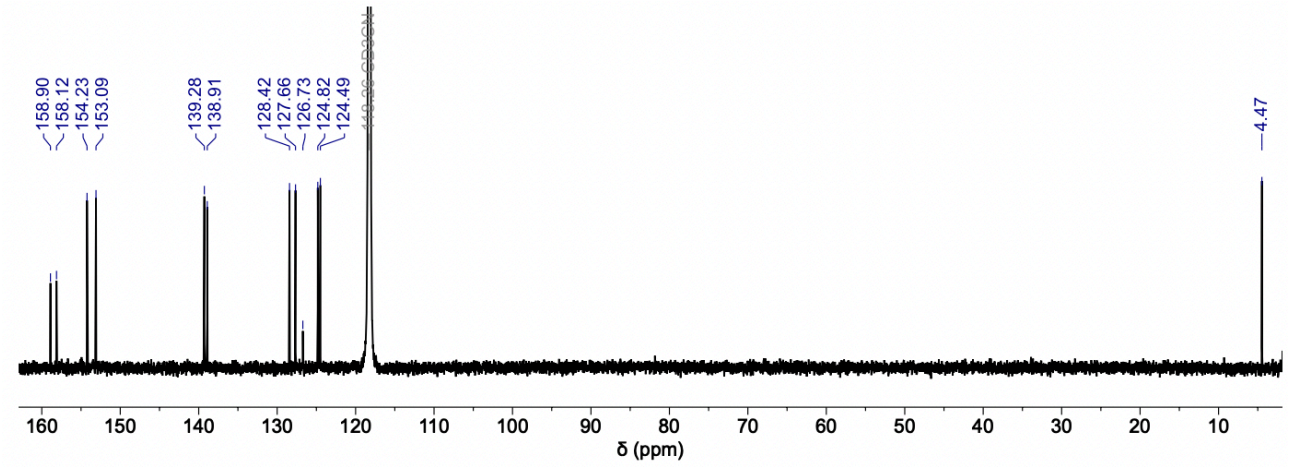

Figure S19. ^{13}C NMR (151 MHz, 298 K, acetonitrile-d_3) spectrum of $[Ru(bpy)_2(MeCN)_2](PF_6)_2$.

S1.7.3 ESI-MS of $[Ru(bpy)_2(MeCN)_2](PF_6)_2$ in acetonitrile

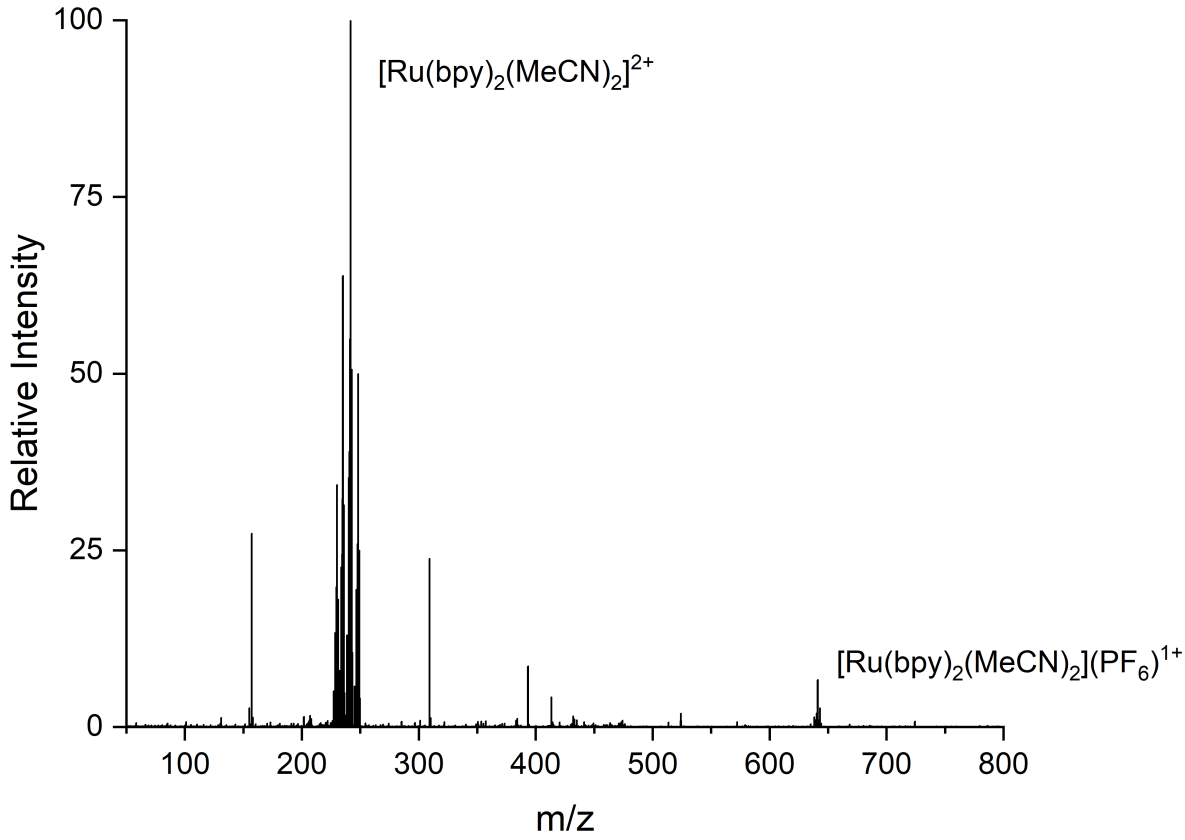

Figure S20. ESI-MS of $[Ru(bpy)_2(MeCN)_2](PF_6)_2$ in acetonitrile.

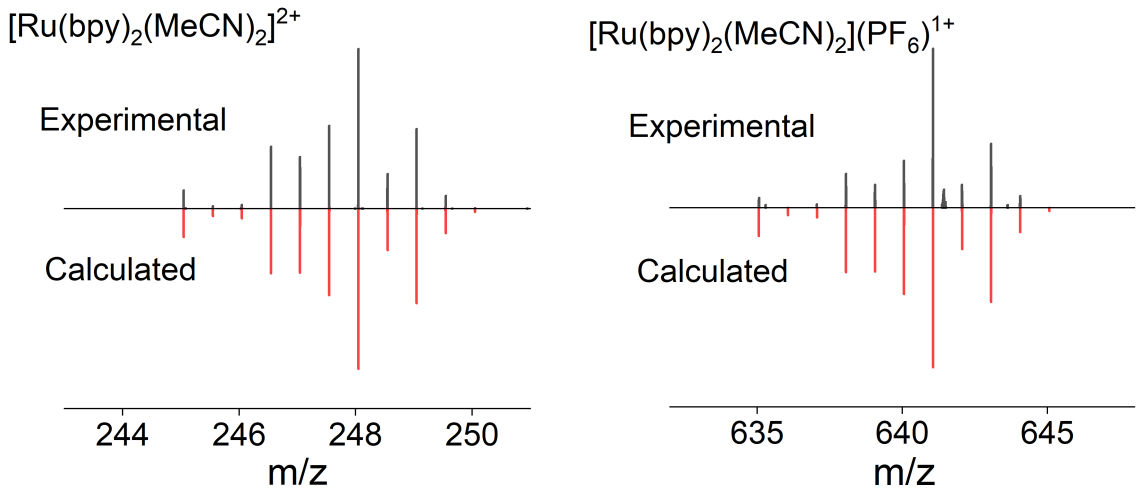

Figure S21. Zoom scans of select ESI-MS peaks, with simulated isotope patterns for $[Ru(bpy)_2(MeCN)_2](PF_6)_2$.

S2. Photoswitching studies of 1

S2.1 Measuring UV-vis spectra of 1 at different PSS in acetonitrile

A sample of **1** in acetonitrile-d_3 was heated in a sand bath at 70 °C overnight to ensure full isomerisation to the *E*-**1** isomer, confirmed by ^{1}H NMR spectroscopy. The sample of *E*-**1** was added dropwise to a quartz cuvette filled with 2.5 mL of acetonitrile until the maximum absorbance of the sample was ~0.95 (Figure S22).

To measure UV-vis absorption spectra at different photostationary states (PSS), the sample was irradiated with LEDs with emissions centred at 365, 425, 470, or 530 nm. For each irradiation wavelength the sample was irradiated until the absorption spectrum was constant. For all irradiation wavelengths, a PSS was reached in under 2 min. Irradiation with 365 nm light produced the highest ratio of the of the *Z* isomer and 530 nm light produced the highest ratio of the *E* isomer.

We calculated the UV-vis absorption spectrum of *Z*-**1** using the UV-vis absorption spectra of ligand **1** and the PSS distributions of *E*-**1** and *Z*-**1** determined using ^{1}H NMR spectroscopy (see S2.2 for details). The absorbance of *Z*-**1** was calculated using the equation:

$$Abs_Z = \frac{Abs_{PSS} - (E \times Abs_E)}{Z}$$

Abs_Z = absorbance of the *Z*-isomer

Abs_{PSS} = absorbance at the relative PSS

E = relative abundance of the *E*-isomer at the PSS, measured by ^{1}H NMR

Abs_E = absorbance of the sample containing all *E*-isomer

Z = relative abundance of the *Z*-isomer at the PSS, measured by ^{1}H NMR

The absorbance of *Z*-**1** was calculated using the absorption spectra for PSS_{365}, PSS_{425}, PSS_{470}, and PSS_{530}. The calculated spectra were averaged, and the standard deviation was calculated and used to estimate errors.

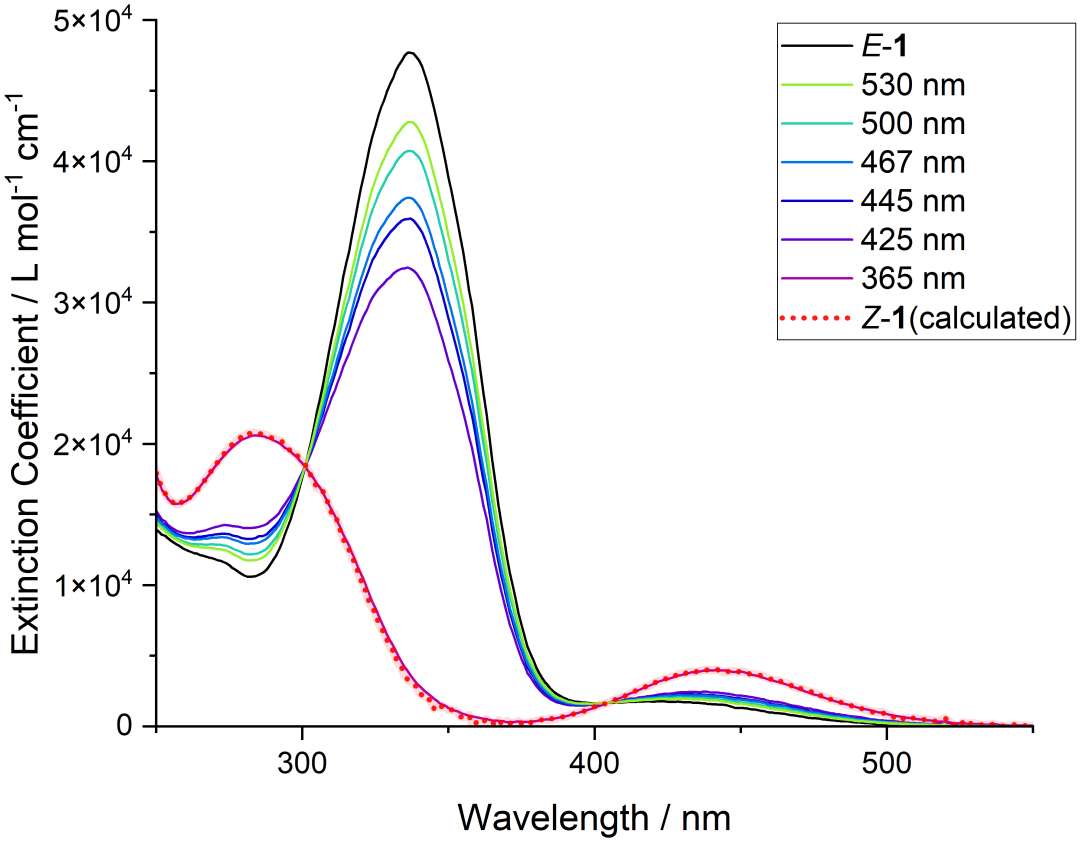

Figure S22. The UV-vis absorption (acetonitrile, 298 K) spectra of **1** at PSS generated using LEDs with emission centered at various wavelengths. The spectrum for *Z*-**1** was calculated using the ^{1}H NMR data together with the absorption spectra solutions at a given PSS when irradiated with 365, 425, 470 and 530 nm light for 2 minutes.

S2.2 Determining the PSS distributions of 1 in acetonitrile-d_3 using ^{1}H NMR spectroscopy

^{1}H NMR spectroscopy was used to determine the distribution of *E*-**1** and *Z*-**1** after generating the PSS at different irradiation wavelengths. A sample of **1** in acetonitrile-d_3 was heated in a sand bath at 70 °C overnight to thermally equilibrate the sample so that only *E*-**1** was present. The sample was irradiated with different LEDs and the ^{1}H NMR spectra monitored until there were no further changes in signal intensities (Figure S23), within 15 minutes for each LED. The sample was irradiated with either 365, 425, 470 or 530 nm light.

The NMR signal integrals for the chemical shifts at 8.51 ppm and 8.41 ppm, corresponding to *E*-**1** H^{A2} and *Z*-**1** H^{A2} were selected as the signals for these environments do not overlap with other signals. After each irradiation period, the relative signal intensities for *E*-**1** and *Z*-**1** were measured, tabulated in Table S2. The relative abundances were used to determine the PSS distribution at PSS_{365} (2:98 *E*:*Z*), PSS_{425} (65:35 *E*:*Z*), PSS_{470} (77:23 *E*:*Z*) PSS_{530} (11:89 *E*:*Z*).

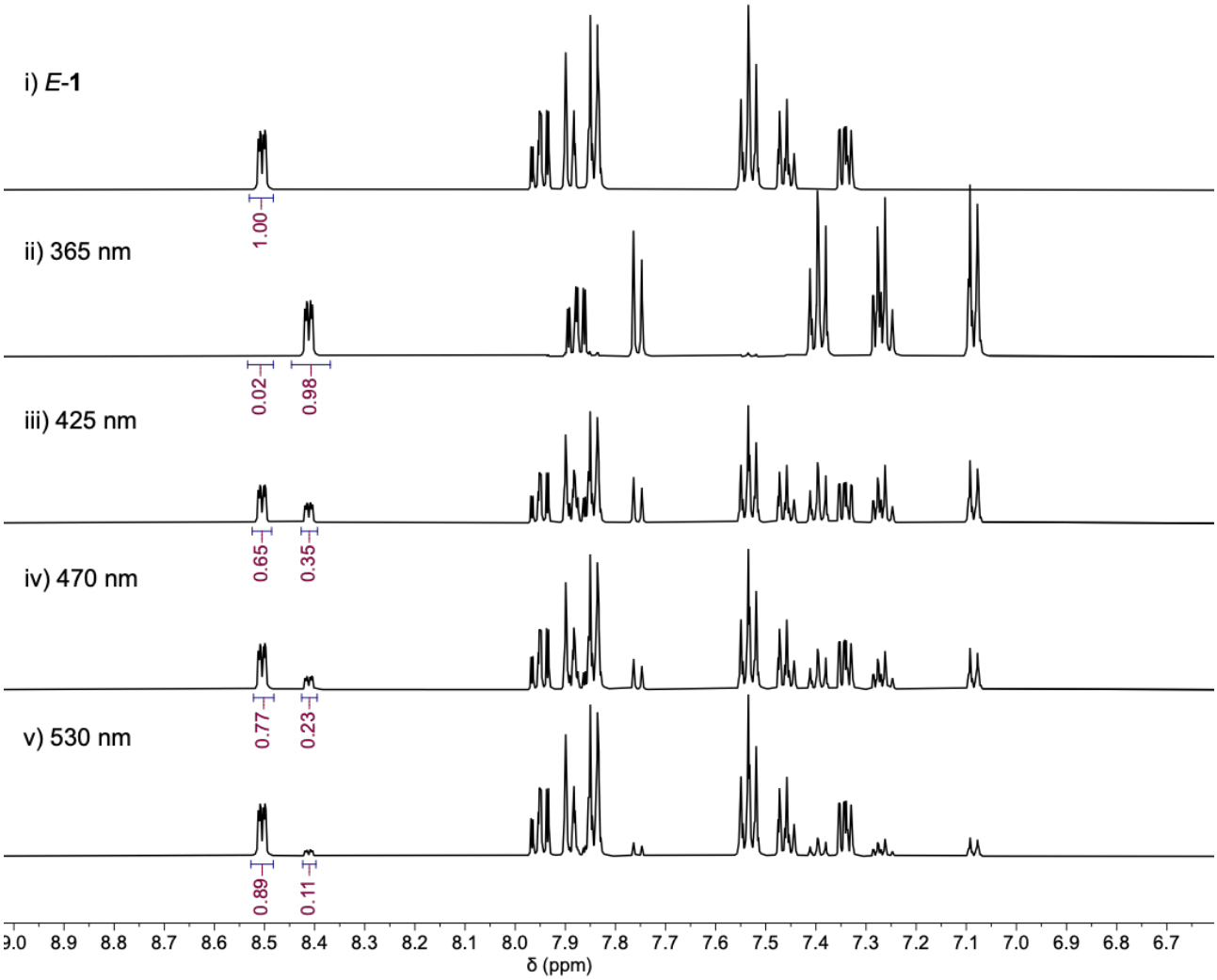

Figure S23. ^{1}H (500 MHz, 298 K, acetonitrile-d_3) NMR spectra of **1** after i) thermal equilibration, after irradiation for 15 minutes with ii) 365 nm light, iii) 425 nm light, iv) 470 nm light, v) 530 nm light.

Table S2. PSS distributions of **1** using different irradiation wavelengths. PSS distributions determined from ^{1}H NMR (500 MHz, 298 K, acetonitrile-d_3).

Irradiation wavelength / nm	%*E*-**1**	%*Z*-**1**
530	89	11
470	77	23
425	65	35
365	2	98

S2.3 Determining the thermal stability of 1 in acetonitrile using UV-vis spectroscopy

UV-vis absorption spectroscopy was used to estimate the thermodynamic parameters for the thermal isomerization of *Z*-**1** to *E*-**1**. The absorbance at 335 nm at 343, 333 and 323 K was monitored to determine the thermal recovery of *E*-**1**. For each temperature, a sample of **1** in acetonitrile was heated to the desired temperature and irradiated with a 365 nm light *in situ* for 2 minutes to enrich the sample in *Z*-**1,** and the absorbance at 335 nm was monitored over 6 hours. The absorbance for each experiment was plotted against time (Figure S24) and the data was fit to a mono-exponential to determine the first-order rate constant (Table S3). Errors were determined from the curve fit.

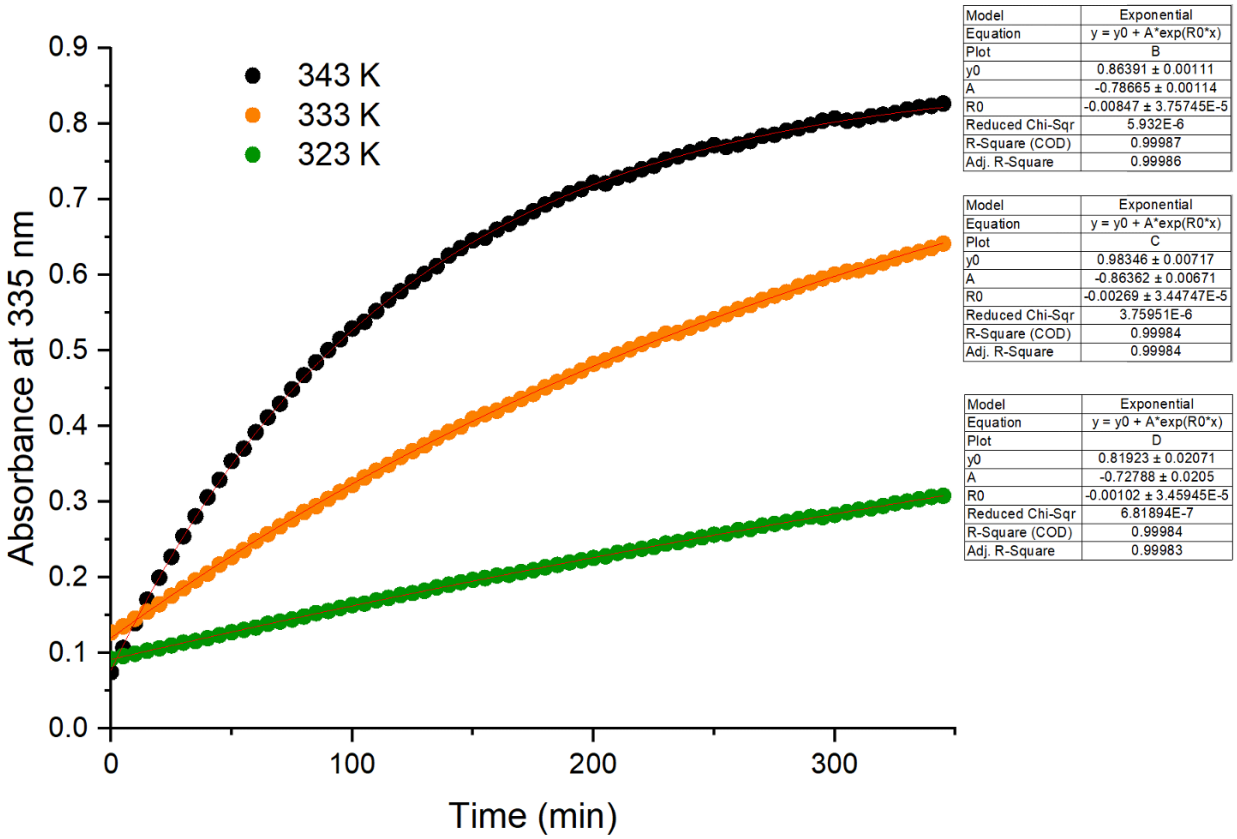

Model	Exponential
Equation	y = y0 + A*exp(R0*x)
Plot	B
y0	0.86391 ± 0.00111
A	-0.78665 ± 0.00114
R0	-0.00847 ± 3.75745E-5
Reduced Chi-Sqr	5.932E-6
R-Square (COD)	0.99987
Adj. R-Square	0.99986

Model	Exponential
Equation	y = y0 + A*exp(R0*x)
Plot	C
y0	0.98346 ± 0.00717
A	-0.86362 ± 0.00671
R0	-0.00269 ± 3.44747E-5
Reduced Chi-Sqr	3.75951E-6
R-Square (COD)	0.99984
Adj. R-Square	0.99984

Model	Exponential
Equation	y = y0 + A*exp(R0*x)
Plot	D
y0	0.81923 ± 0.02071
A	-0.72788 ± 0.0205
R0	-0.00102 ± 3.45945E-5
Reduced Chi-Sqr	6.81894E-7
R-Square (COD)	0.99984
Adj. R-Square	0.99983

Figure S24. Thermal isomerization of *Z*-**1** to *E*-**1** in acetonitrile at 343, 333, and 323 K. Monitored by UV-vis absorption at 335 nm.

Table S3. First-order rate constants for the thermal isomerization of *Z*-**1** to *E*-**1** at different temperatures.

Temperature / K	343	333	323
k / min^{-1} × 10^{-3}	8.47 ± 0.04	2.69 ± 0.03	1.02 ± 0.03
k / s^{-1} × 10^{-4}	1.41 ± 0.006	0.448 ± 0.006	0.170 ± 0.006
ln(k/T)	−14.7 ± 0.2	-15.8 ± 0.2	−168 ± 0.2
1/T / K^{-1} × 10^{-3}	2.92 ± 0.008	3.03 ± 0.008	3.10 ± 0.008

The first-order rate constants were determined in acetonitrile by fitting the absorbance data to a mono-exponential function. An Eyring plot (Figure S25) was used to estimate the entropy of activation ($\Delta S^{\ddagger}$ = −44.3 J·mol^{-1}·K^{-1}), and the enthalpy of activation ($\Delta H^{\ddagger}$ = 94.6 kJ·mol^{-1}). Using these parameters, the change in Gibbs free energy of activation, $\Delta G^{\ddagger}$, for thermal isomerisation of **1** was calculated for each temperature (Table S4). The extrapolation from the Eyring plot (Table S5) assumes that $\Delta H^{\ddagger}$ and $\Delta S^{\ddagger}$ remain constant across all temperatures and therefore the mechanism does not vary with temperature, which is likely reasonable for the intramolecular isomerization reaction. The values determined using the Eyring plot were extrapolated to determine $\Delta G^{\ddagger}$ and the half-life at 298 K for the thermal isomerisation of **1**.

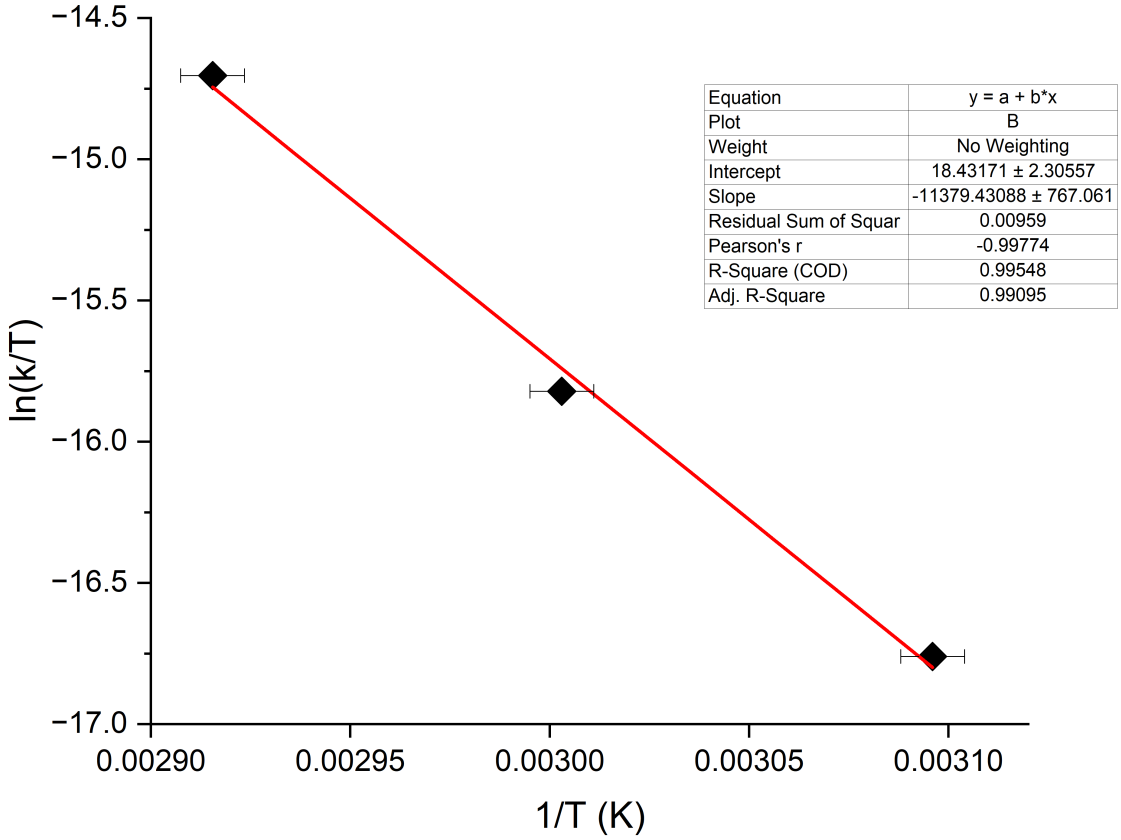

Figure S25. Eyring plot for the thermal isomerization of *Z*-**1** to *E*-**1** in acetonitrile. Rate constants (Table S3) were determined using UV-vis spectroscopy at 343, 333, 323 K (Table S4).

Table S4. $\Delta G^{\ddagger}$ for the thermal isomerization of *Z*-**1** to *E*-**1** in acetonitrile at different temperatures.

Temperature / K	343	333	323
$\Delta G^{\ddagger}$ / kJ·mol^{-1}	79.4 ± 7.2	79.9 ± 7.0	80.3 ± 6.9

Table S5. Thermodynamic parameters and half-life for the thermal isomerization of *Z*-**1** to *E*-**1** in acetonitrile at 298 K.

$\Delta G^{\ddagger}$ / kJ·mol^{-1}	$\Delta H^{\ddagger}$ / kJ·mol^{-1}	$\Delta S^{\ddagger}$ / kJ·mol^{-1}	$t_{½}$ / days
110.2 ± 8.6	94.6 ± 6.3	44.3 ± 2.3	10

S2.4 Determining the PSS distribution of 1 in a solution of 1 and $[Ru(bpy)_3](PF_6)_2$ in acetonitrile-d_3 using ^{1}H NMR spectroscopy

^{1}H NMR spectroscopy was used to determine the distribution of *E*-**1** and *Z*-**1** with $[Ru(bpy)_3](PF_6)_2$ after generating the PSS at 365 nm. A sample of **1** in acetonitrile-d_3 was heated in a sand bath at 70 °C overnight to thermally equilibrate the sample so that only *E*-**1** was present. $[Ru(bpy)_3](PF_6)_2$ (1 equiv.) was added. The method followed below is the same as in S2.2 . The sample was irradiated with 365 nm light and the ^{1}H NMR spectra was monitored until no further changes in signal intensities were detected, which was after 30 minutes.

The NMR signal integrals for the chemical shifts at 2.99 ppm and 1.62 ppm, corresponding to *E*-**1** H^{B2} and *Z*-**1** H^{B2} were selected as the signals for these environments do not overlap with other signals. The relative signal intensities for *E*-**1** and *Z*-**1** were measured and used to determine the PSS distribution of 52:48 *E*:*Z* for **1** with $[Ru(bpy)_3](PF_6)_2$. This differs from **1** alone which has a PSS distribution of 2:98 *E*:*Z* under identical irradiation conditions.

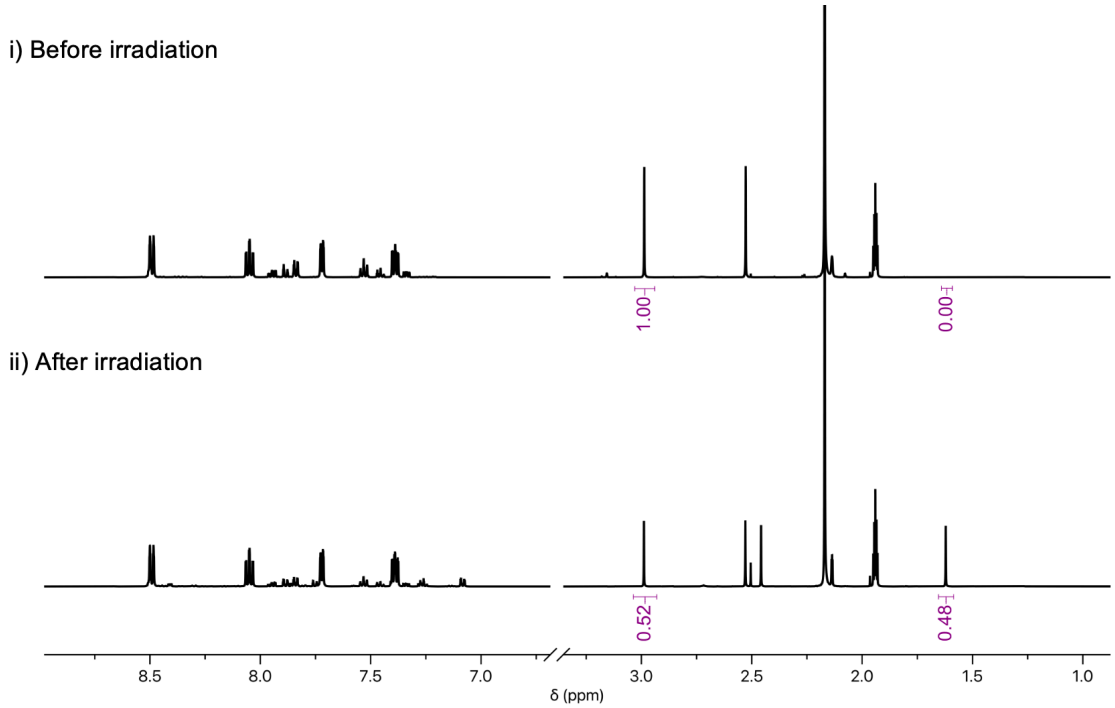

Figure S26. ^{1}H (500 MHz, 298 K, acetonitrile-d_3) NMR spectra of **1** and $[Ru(bpy)_3](PF_6)_2$ i) in the dark and ii) after irradiation with 365 light for 30 minutes.

S3. Behaviour of [Ru(bpy)$_2$(*E*-1)](PF$_6$)$_2$ under irradiation monitored by UV-vis spectroscopy

S3.1 Irradiation studies of [Ru(bpy)$_2$(*E*-1)](PF$_6$)$_2$ via UV-vis spectroscopy

The UV-vis absorption spectra of [Ru(bpy)$_2$(*E*-**1**)](PF$_6$)$_2$ was determined at different irradiation wavelengths (Figure S27). For each irradiation wavelength, a new sample of [Ru(bpy)$_2$(*E*-**1**)](PF$_6$)$_2$ (13 μM, acetonitrile, 298 K) was irradiated with 530 nm, 445 nm, or 365 nm light for 25 minutes.

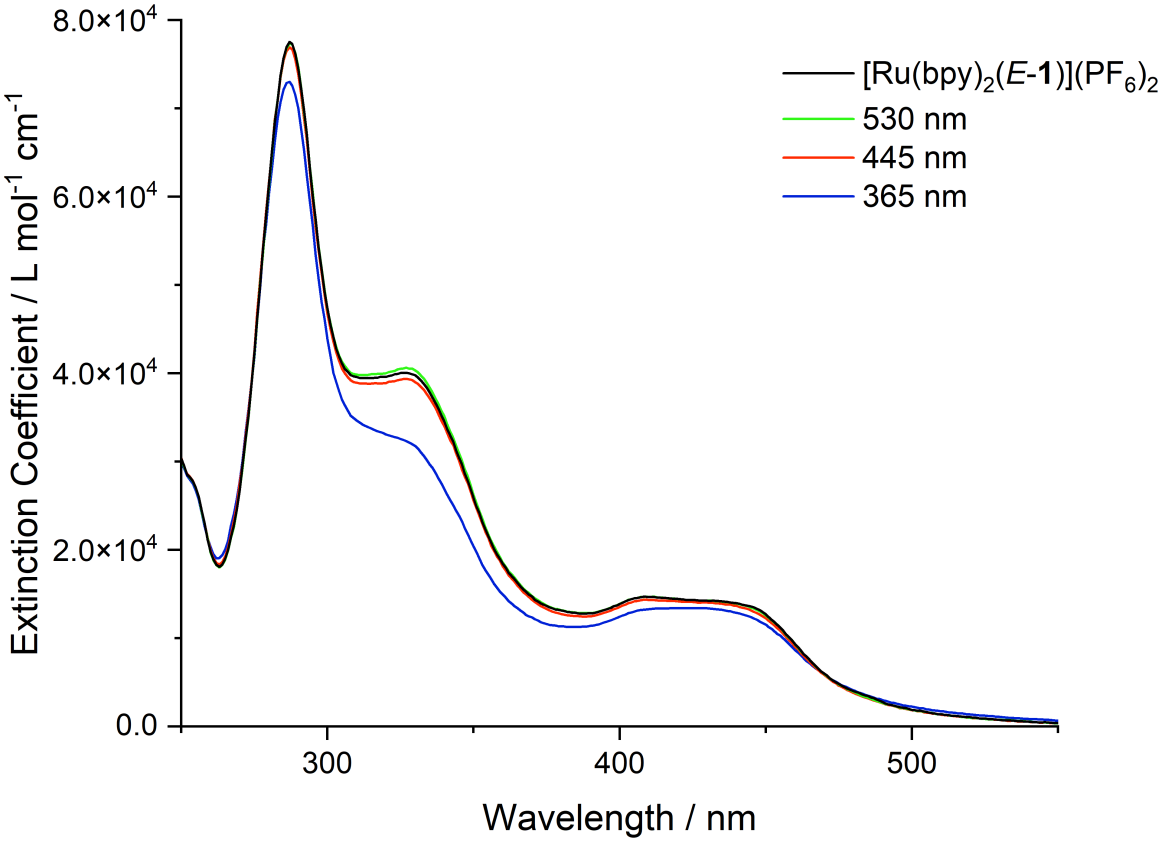

Figure S27. The UV-vis absorption spectra of [Ru(bpy)$_2$(*E*-**1**)](PF$_6$)$_2$ (13 μM, acetonitrile, 298 K) in the dark and after irradiation with LEDs centered at 365 nm, 445 nm or 530 nm for 25 minutes.

The UV-vis absorption for [Ru(bpy)$_2$(*E*-**1**)](PF$_6$)$_2$ changes less than 2% when irradiated with 445 nm light with the greatest change in absorption occurring at 330 nm. The absorption changes less than 1.5% when irradiated with 530 nm light with the greatest change occurring at 333 nm.

The changes in the UV-vis absorption when irradiated with 365 nm light with a maximum of 21% change in the absorption at 334 nm, which coincides with the absorbance change when *E*-**1** undergoes photoswitching to *Z*-**1** (Figure S22).

S3.2 Irradiation studies of [Ru(bpy)$_2$(2)](PF$_6$)$_2$

The UV-vis absorption spectra of [Ru(bpy)$_2$(**2**)](PF$_6$)$_2$ were measured under irradiation with different wavelengths LEDs (Figure S28). For each irradiation wavelength, a new sample of [Ru(bpy)$_2$(**2**)](PF$_6$)$_2$ (10 μM, acetonitrile, 298 K) was irradiated with 530 nm, 445nm, or 365 nm light for 25 minutes each.

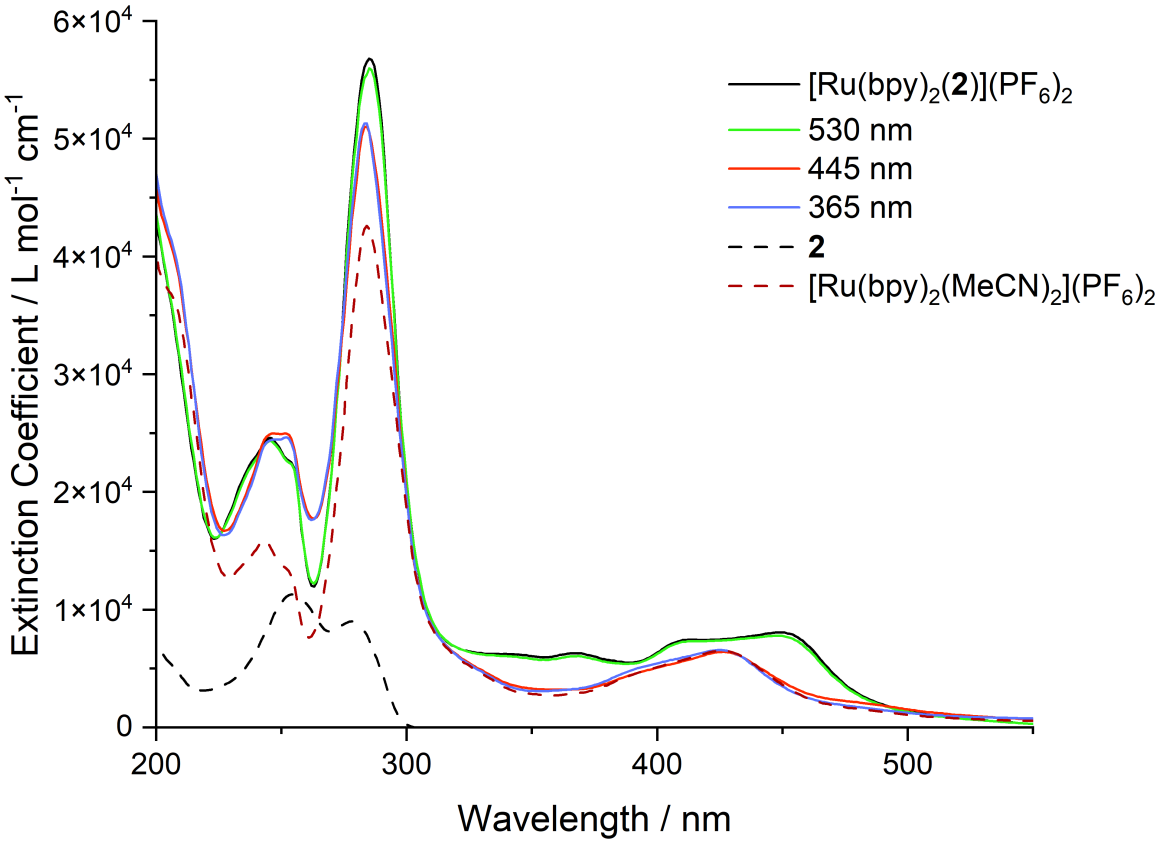

Figure S28. The UV-vis absorption (10 μM, acetonitrile, 298 K) spectra of $[Ru(bpy)_2(\mathbf{2})](PF_6)_2$ in the dark and after irradiation at 365 nm, 445 nm and 530 nm light for 25 minutes. The UV-vis spectra of **2** and $[Ru(bpy)_2(MeCN)_2](PF_6)_2$ are also shown with dashed lines.

After irradiation with 530 nm, the UV-vis absorption of $[Ru(bpy)_2(\mathbf{2})](PF_6)_2$ changes less than 1.5% from measurements taken in the dark with the greatest difference being at the λ_{max} (285 nm) of the complex. The absorption changes are more significant after irradiation with 445 nm light and 365 nm light with these changes being 52% and 56% decrease in absorbance intensity for each irradiation wavelength respectively.

After irradiation with 365 nm light, the UV-vis spectrum matches that of $[Ru(bpy)_2(MeCN)_2](PF_6)_2$ above 300 nm. This is expected if $[Ru(bpy)_2(\mathbf{2})](PF_6)_2$ ejects **2** to form $[Ru(bpy)_2(MeCN)_2](PF_6)_2$ and **2** does not absorb above 300 nm. The UV-vis spectrum of $[Ru(bpy)_2(\textit{E}\text{-}\mathbf{1})](PF_6)_2$ did not match the absorption spectra of $[Ru(bpy)_2(MeCN)_2](PF_6)_2$ when irradiated with 365 nm light (Figure S27).

S3.3 Irradiation with 365 nm light of $[Ru(bpy)_2(\textit{E}\text{-}\mathbf{1})](PF_6)_2$ monitored by UV-vis spectroscopy

A sample of $[Ru(bpy)_2(\textit{E}\text{-}\mathbf{1})](PF_6)_2$ (13 μM, acetonitrile, 298 K) was irradiated at 365 nm and the absorbance was monitored over 81 minutes (Figure S29).

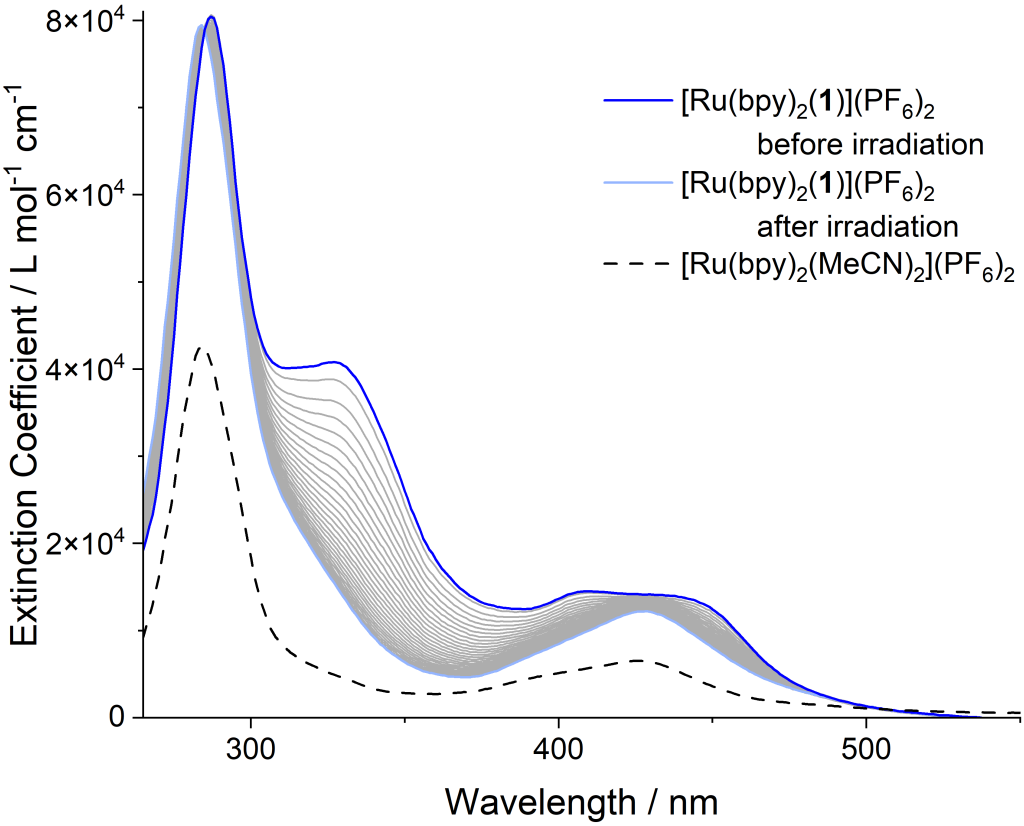

Figure S29. UV-vis absorption spectra of $[Ru(bpy)_2(\mathbf{1})](PF_6)_2$ (13 μM, acetonitrile, 298 K) after irradiation at 365 nm for 75 minutes. From 0 minutes (dark blue) to 75 minutes (light blue). UV-vis absorption spectra of $[Ru(bpy)_2(MeCN)_2](PF_6)_2$ is shown through a dashed line.

The absorption continued to change over 75 min, with a decrease at 340 nm where the absorption of **1** decreases from the *E*-**1** to the *Z*-**1** form. As discussed in S3.1 , this is consistent with the photoswitching of **1** occurring either while attached to the ruthenium centre to form $[Ru(bpy)_2(Z\text{-}\mathbf{1})](PF_6)_2$, or where **1** is first ejected from the ruthenium centre and forms *Z*-**1** in free solution.

A sample of $[Ru(bpy)_2(E\text{-}\mathbf{1})](PF_6)_2$ (10 μM, acetonitrile, 298 K) in acetonitrile was irradiated at 365 nm for 75 mins, then heated at 75 C and monitored via UV-vis spectroscopy. After 81 min of heating the spectrum did not return to the absorption spectrum of $[Ru(bpy)_2(E\text{-}\mathbf{1})](PF_6)_2$ in the dark (Figure S30). The absorption increases in the 300 – 375 nm range.

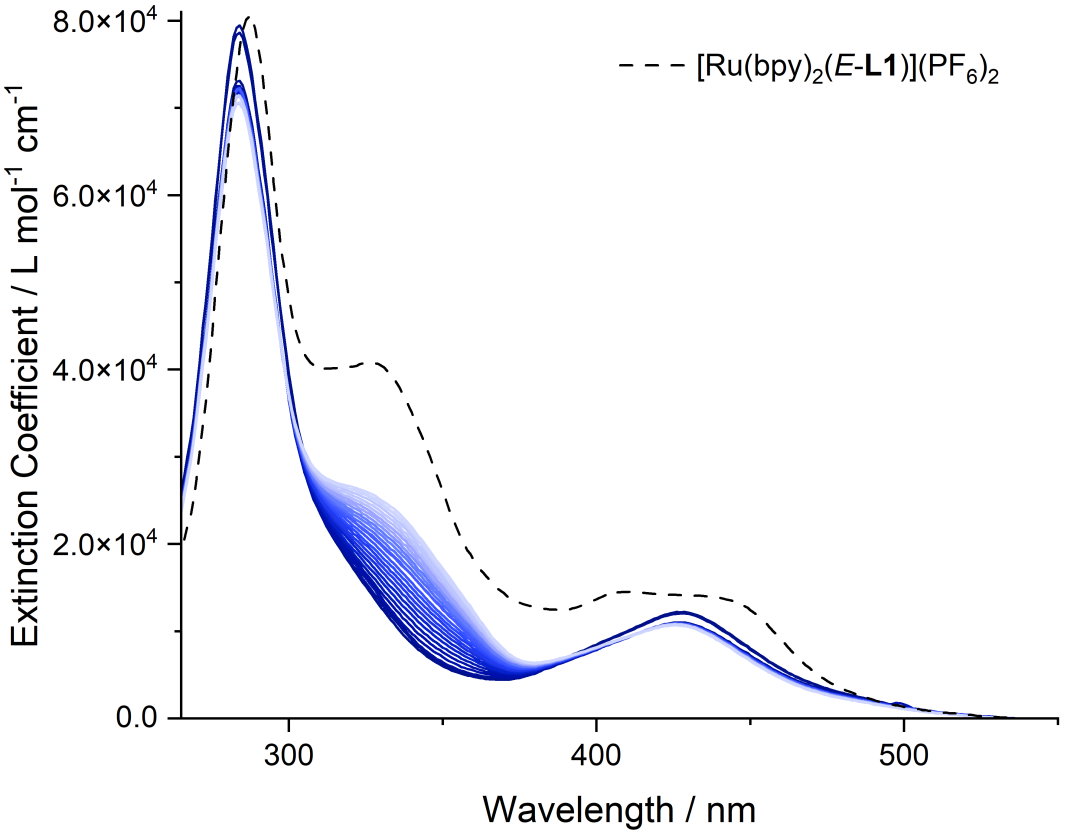

Figure S30. The UV-vis absorption (acetonitrile, 298 K) spectra of $[Ru(bpy)_2(E\text{-}\mathbf{1})](PF_6)_2$ after irradiation at 365 nm after heating at 75 C for 81 minutes. 0 minutes dark blue to 81 minutes light blue. Dashed line represents the UV-vis spectra of $[Ru(bpy)_2(E\text{-}\mathbf{1})](PF_6)_2$ in the dark.

S3.4 Irradiation with 365 nm light of $[Ru(bpy)_2(2)](PF_6)_2$ monitored by UV-vis spectroscopy

A sample of $[Ru(bpy)_2(\mathbf{2})](PF_6)_2$ (10 μM, acetonitrile, 298 K) was irradiated at 365 nm and the absorbance was monitored over 75 minutes (Figure S31).

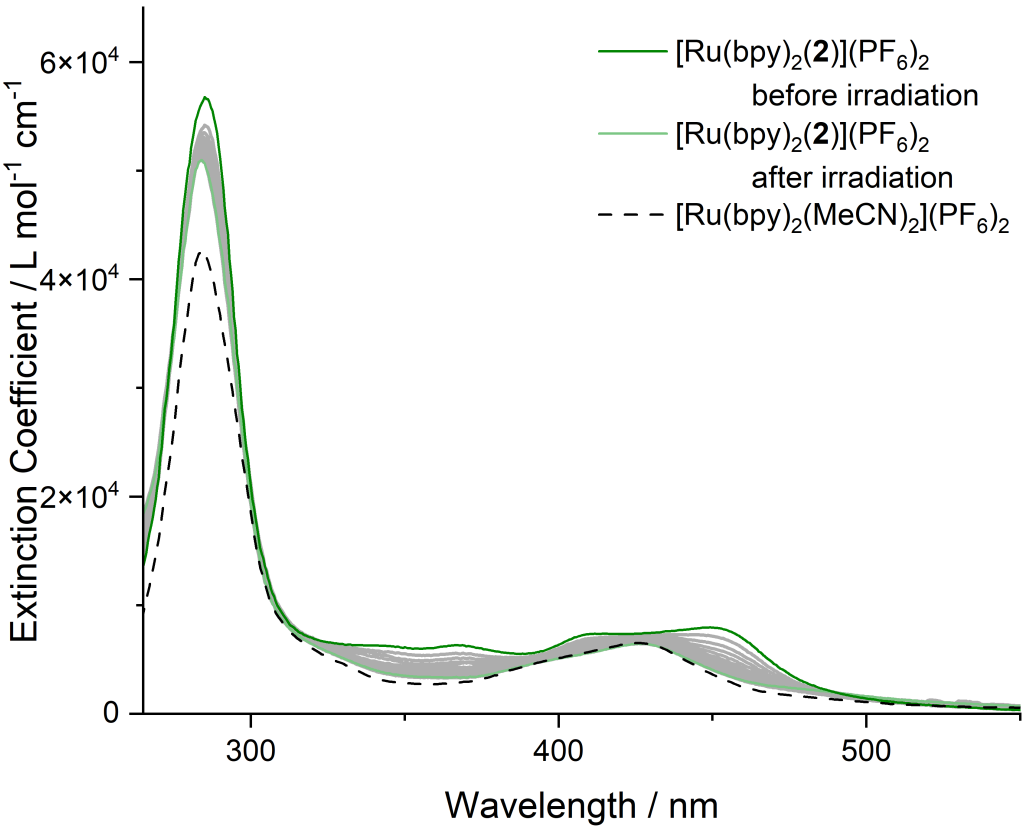

Figure S31. The UV-vis absorption (10 μM, acetonitrile, 298 K) spectra of $[Ru(bpy)_2(\mathbf{2})](PF_6)_2$ after irradiation at 365 nm for 75 minutes. 0 minutes dark green to 75 minutes light blue.

The change in absorbance over 75 minutes of $[Ru(bpy)_2(\mathit{E}\text{-}\mathbf{1})](PF_6)_2$ and $[Ru(bpy)_2(\mathbf{2})](PF_6)_2$ was compared to the absorbance of the ejected compound, $[Ru(bpy)_2(MeCN)_2](PF_6)_2$ (Figure S32). The change in absorbance at 450 nm was chosen as this where **1** has a low absorbance (Figure S22) and therefore while some change in absorption may arise from the photoswitching of **1**, the difference is less significant than the difference between the absorption of $[Ru(bpy)_2(\mathit{E}\text{-}\mathbf{1})](PF_6)_2$ and $[Ru(bpy)_2(MeCN)_2](PF_6)_2$.

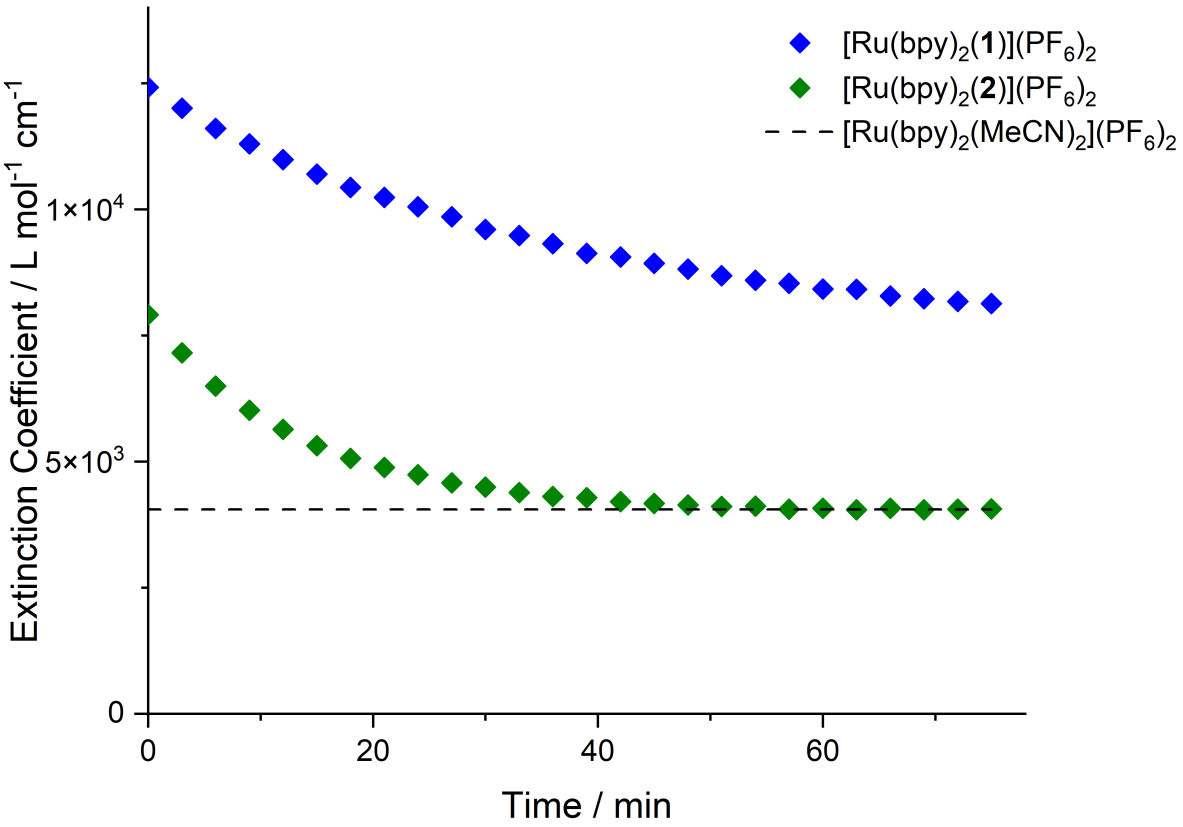

Figure S32. Extinction coefficient at 450 nm of $[Ru(bpy)_2(E\text{-}\mathbf{1})](PF_6)_2$ and $[Ru(bpy)_2(\mathbf{2})](PF_6)_2$ (acetonitrile, 298 K) during irradiation with 365 nm light for 75 minutes. $[Ru(bpy)_2(MeCN)_2](PF_6)_2$ is shown through a dashed line.

After an acetonitrile solution of $[Ru(bpy)_2(\mathbf{2})](PF_6)_2$ was irradiated with 365 nm light for 75 min, the extinction coefficient at 450 nm matches of $[Ru(bpy)_2(MeCN)_2](PF_6)_2$. This is not the same for $[Ru(bpy)_2(E\text{-}\mathbf{1})](PF_6)_2$.

S4. Behaviour of [Ru(bpy)$_2$(*E*-1)](PF$_6$)$_2$ with irradiation with 365 nm light monitored by NMR spectroscopy

S4.1 Irradiation with 365 nm light for [Ru(bpy)$_2$(*E*-1)](PF$_6$)$_2$ monitored by NMR spectroscopy

A ^{1}H NMR spectrum of [Ru(bpy)$_2$(*E*-**1**)](PF$_6$)$_2$ in acetonitrile-d_3 was measured in the dark and after being irradiated with 365 nm light for 30 minutes, 1.5 hours and 2.5 hours (Figure S33). The major species (making up 76% of the signal intensity for the mixture per proton) that remains after prolonged irradiation is [Ru(bpy)$_2$(*E*-**1**)](PF$_6$)$_2$. New peaks at 8.43, 8.33, 7.98, 7.92, 7.72, 7.16, 6.86, 2.85 and 0.68 ppm increase in intensity with increased irradiation time (Figure S33 in red). Experiments to separate this new species via TLC and column were unsuccessful, suggesting that this new species has a similar polarity to [Ru(bpy)$_2$(*E*-**1**)](PF$_6$)$_2$.

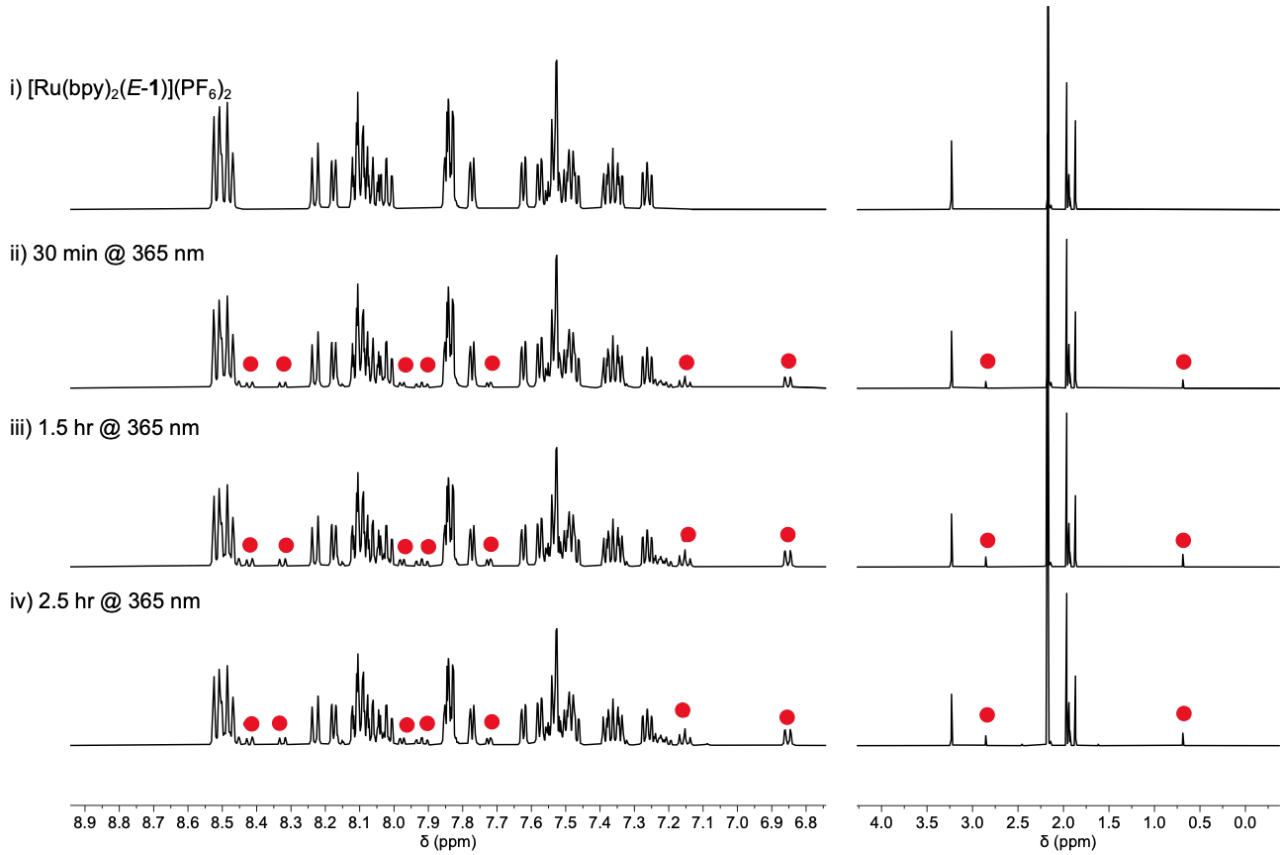

Figure S33. ^{1}H (500 MHz, 298 K, acetonitrile-d_3) NMR spectra of [Ru(bpy)$_2$(*E*-**1**)](PF$_6$)$_2$ i) in the dark and after irradiation at 365 nm for ii) 30 mins, iii) 1.5 hours, and iv) 2.5 hours. New peaks are notated in red.

New peaks with lower intensity (making up 4.7% of the signal intensity for the mixture per proton, such as those at 9.30 ppm and 8.36 ppm (shown in blue in Figure S34) are typical for H^{D6} and H$^{D3'}$ of [Ru(bpy)$_2$(MeCN)$_2$](PF$_6$)$_2$ (Figure S17) indicating the formation of this complex. Peaks at 2.45 and 1.62 ppm (shown in green in Figure S34) are typical for H^{B2} and H^{B5} of the free *Z*-**1** ligand, indicating the formation of this compound.

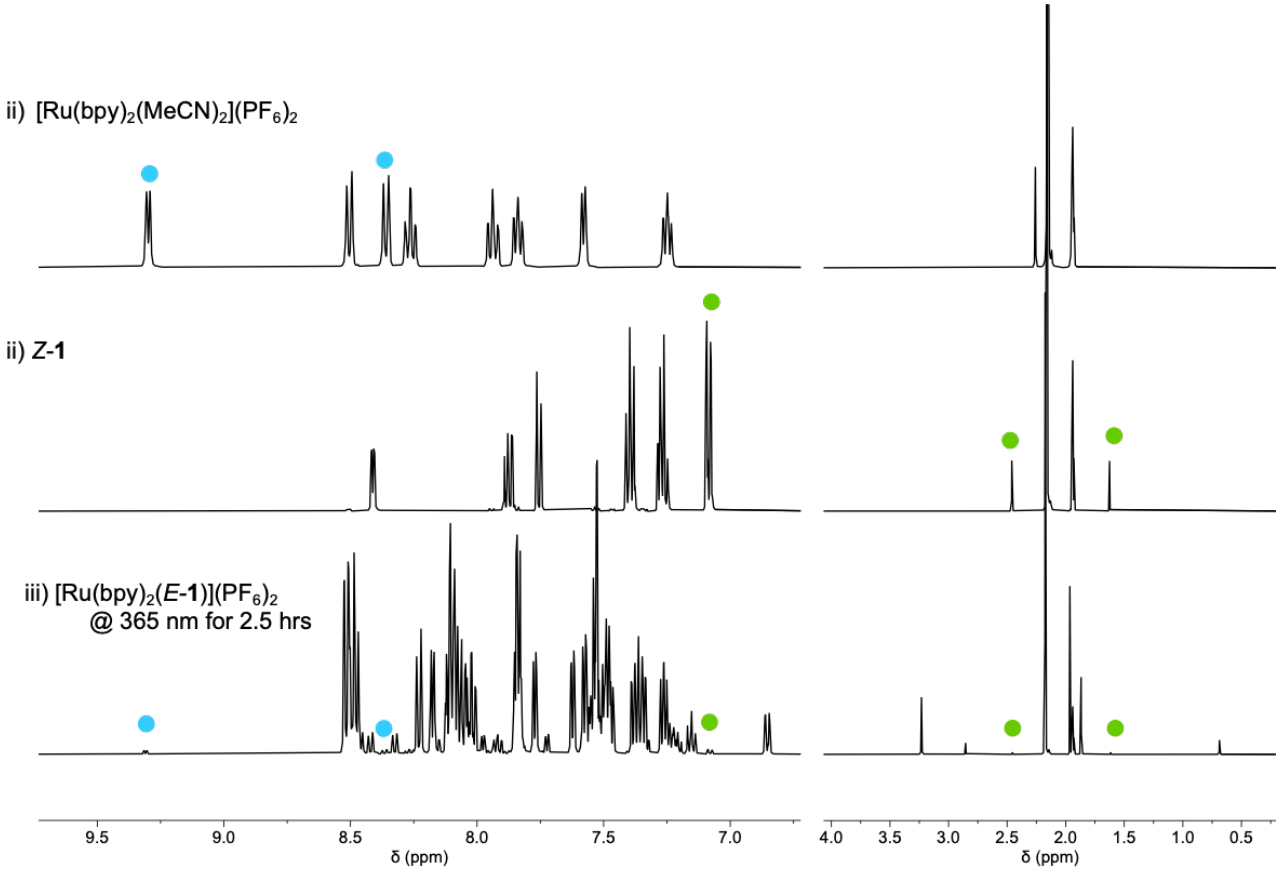

Figure S34. ^{1}H (500 MHz, 298 K, acetonitrile-d_3) NMR spectra of i) $[Ru(bpy)_2(MeCN)_2](PF_6)_2$, ii) *Z*-**1**, iii) $[Ru(bpy)_2(E\text{-}\mathbf{1})](PF_6)_2$ after irradiation at 365 nm for 2.5 hours. Peaks in iii) due to $[Ru(bpy)_2(MeCN)_2](PF_6)_2$ are shown in blue and peaks forming due to *Z*-**1** are shown in green.

S4.2 Irradiation with 365 nm light for of $[Ru(bpy)_2(2)](PF_6)_2$ monitored by NMR spectroscopy

A ^{1}H NMR spectrum of a sample of $[Ru(bpy)_2(\mathbf{2})](PF_6)_2$ in acetonitrile-d_3 was measured in the dark and after being irradiated by 365 nm light for 30 minutes (Figure S35). After 30 minutes of irradiation at 365 nm, the sample contains all signals that are typical for $[Ru(bpy)_2(MeCN)_2](PF_6)_2$ and **2** indicating the formation of these two species.

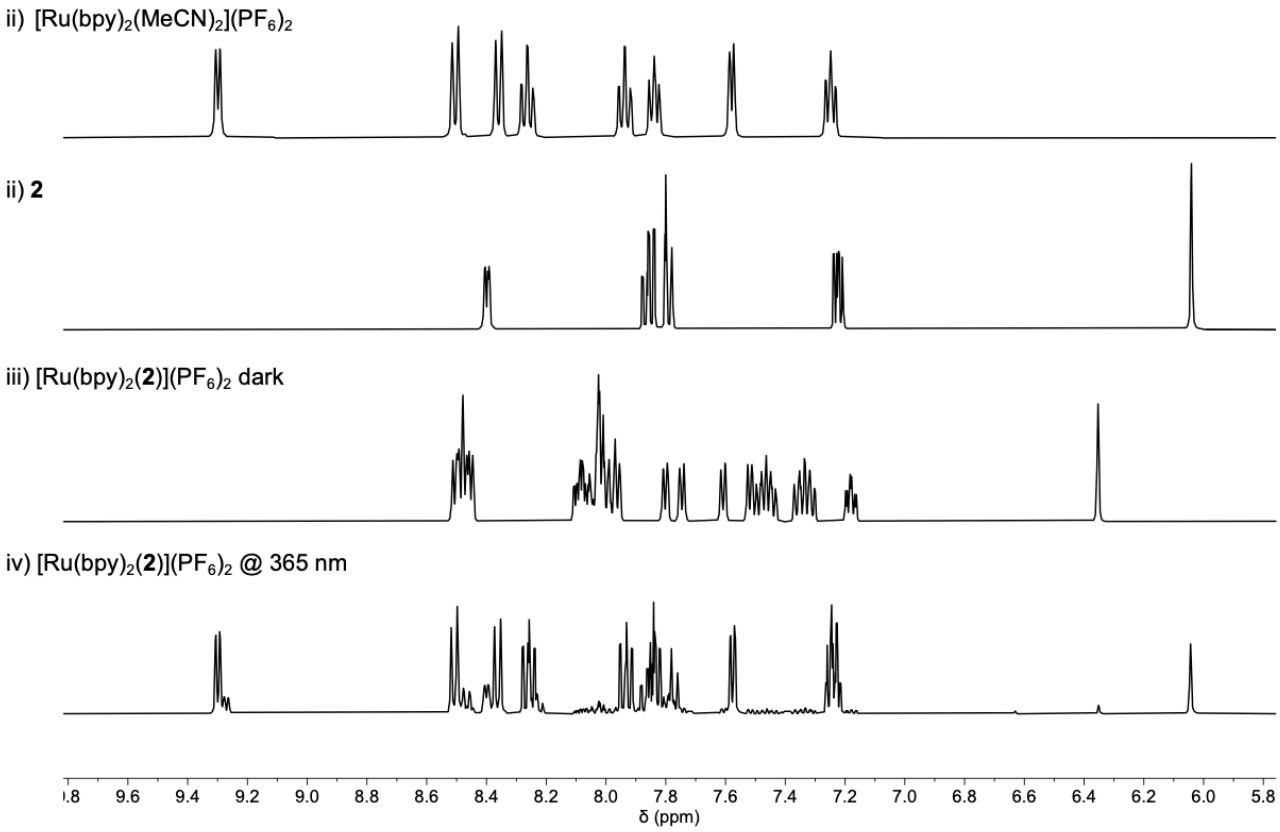

Figure S35. ^{1}H (500 MHz, 298 K, acetonitrile-d_3) NMR spectra of i) $[Ru(bpy)_2(MeCN)_2](PF_6)_2$, ii) **2**, iii) $[Ru(bpy)_2(\mathbf{2})](PF_6)_2$, and iv) $[Ru(bpy)_2(\mathbf{2})](PF_6)_2$ after irradiation at 365 nm for 30 mins.

S4.3 Heating irradiated [Ru(bpy)$_2$(*E*-1)](PF$_6$)$_2$ monitored by NMR spectroscopy

A sample of [Ru(bpy)$_2$(*E*-**1**)](PF$_6$)$_2$ in acetonitrile-d_3 was irradiated by 365 nm light for 3.5 hours and heated at 75 °C for 5 hours (Figure S36). The new peaks that form when [Ru(bpy)$_2$(*E*-**1**)](PF$_6$)$_2$ is irradiated (highlighted in Figure S36), reduce in intensity when heated.

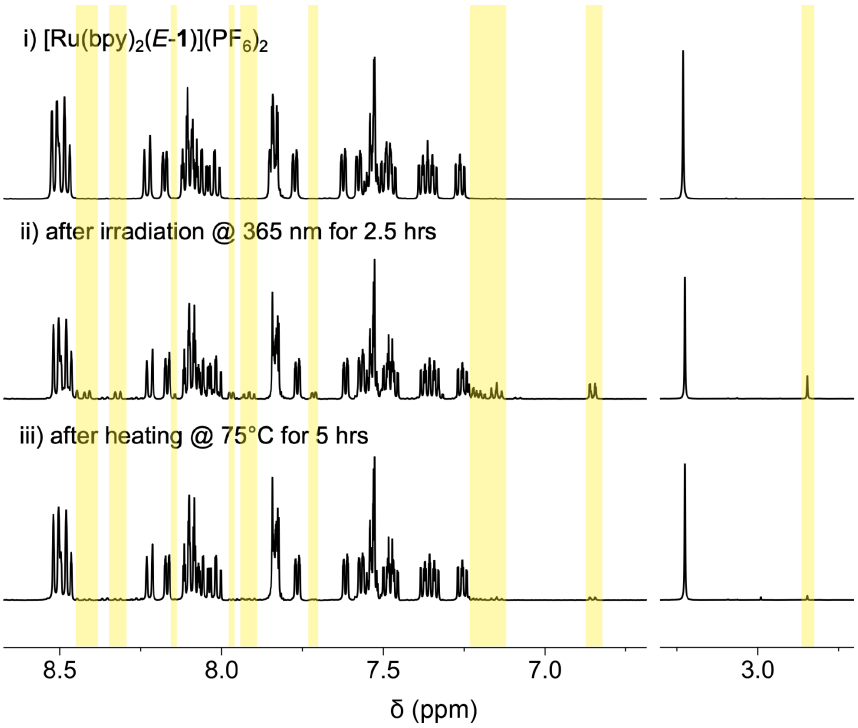

Figure S36. ^{1}H (500 MHz, 298 K, acetonitrile-d_3) NMR spectra of [Ru(bpy)$_2$(*E*-**1**)](PF$_6$)$_2$ after i) irradiation for 3.5 hours ii) heating at 75 C for 5 hours. Peaks of interest are highlighted.

S4.4 Heating $[Ru(bpy)_2(MeCN)_2](PF_6)_2$ and *Z*-1 monitored by NMR spectroscopy

A ^{1}H NMR spectrum of a sample of $[Ru(bpy)_2(MeCN)_2](PF_6)_2$ and *Z*-**1** in a 1:1 molar ratio in acetonitrile-d_3 was measured in the dark, and after being heating at 50 °C for 1.75 hours (Figure S37). Only the peaks corresponding to $[Ru(bpy)_2(MeCN)_2](PF_6)_2$ and *Z*-**1** were observed, as well as smaller intensity peaks characteristic of *E*-**1**. No new peaks were detected.

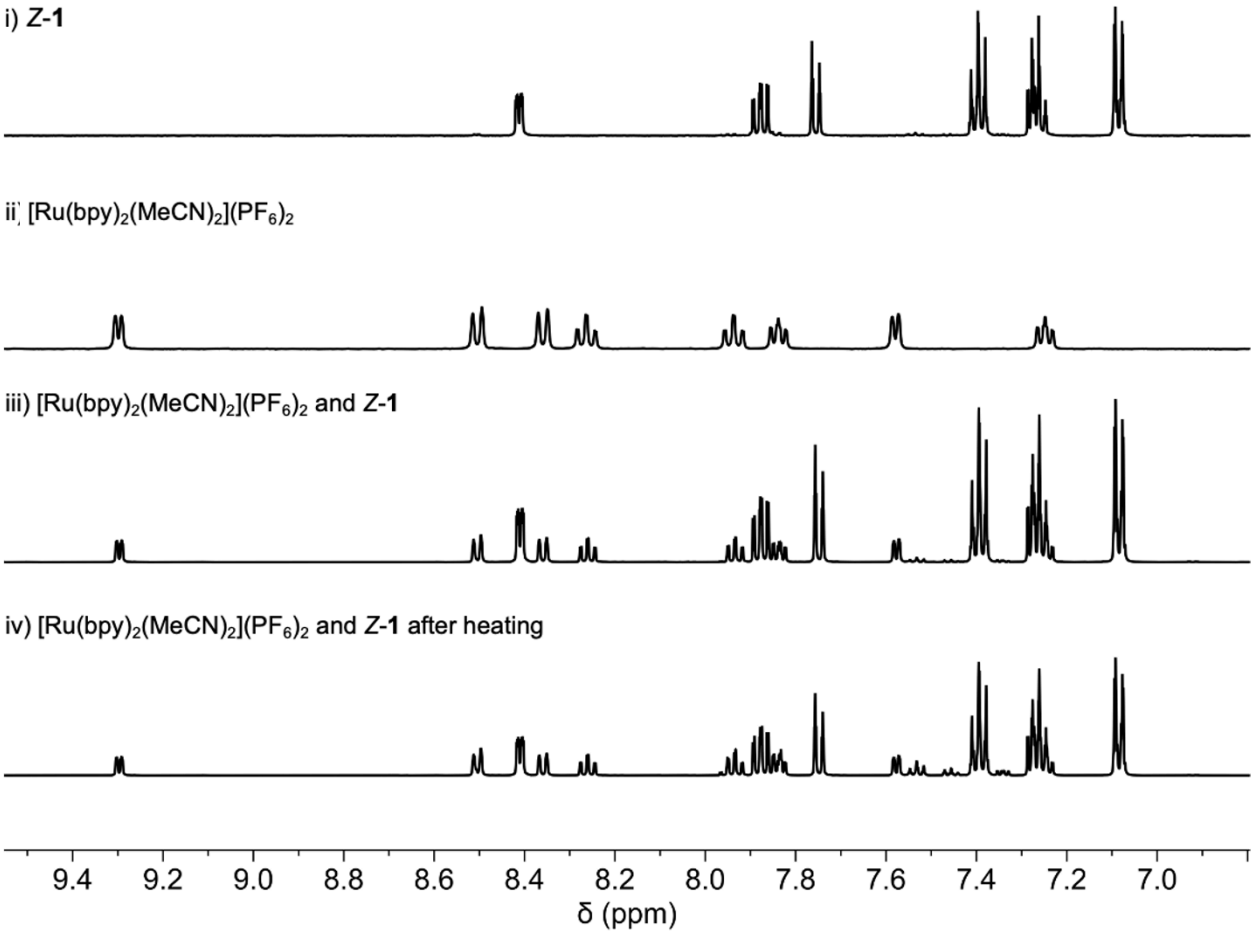

Figure S37. ^{1}H (500 MHz, 298 K, acetonitrile-d_3) NMR spectra of i) *Z*-**1**, ii) $[Ru(bpy)_2(MeCN)_2](PF_6)_2$, iii) $[Ru(bpy)_2(MeCN)_2](PF_6)_2$ and *Z*-**1** in a 1:1 ratio, iv) $[Ru(bpy)_2(MeCN)_2](PF_6)_2$ and *Z*-**1** after heating for 1.75 hours at 50 °C.

S4.5 Heating $[Ru(bpy)_2(MeCN)_2](PF_6)_2$ and *E*-1 monitored by NMR spectroscopy

A ^{1}H NMR spectrum of a sample of $[Ru(bpy)_2(MeCN)_2](PF_6)_2$ and *E*-**1** in a 1:1 molar ratio in acetonitrile-d_3 was measured in the dark, and after being heating at 50 °C for 1.75 hours (Figure S38). Only the peaks corresponding to $[Ru(bpy)_2(MeCN)_2](PF_6)_2$ and *E*-**1** could be seen and no new peaks characteristic of $[Ru(bpy)_2(E\text{-}\mathbf{1})](PF_6)_2$ or any other new peaks were detected.

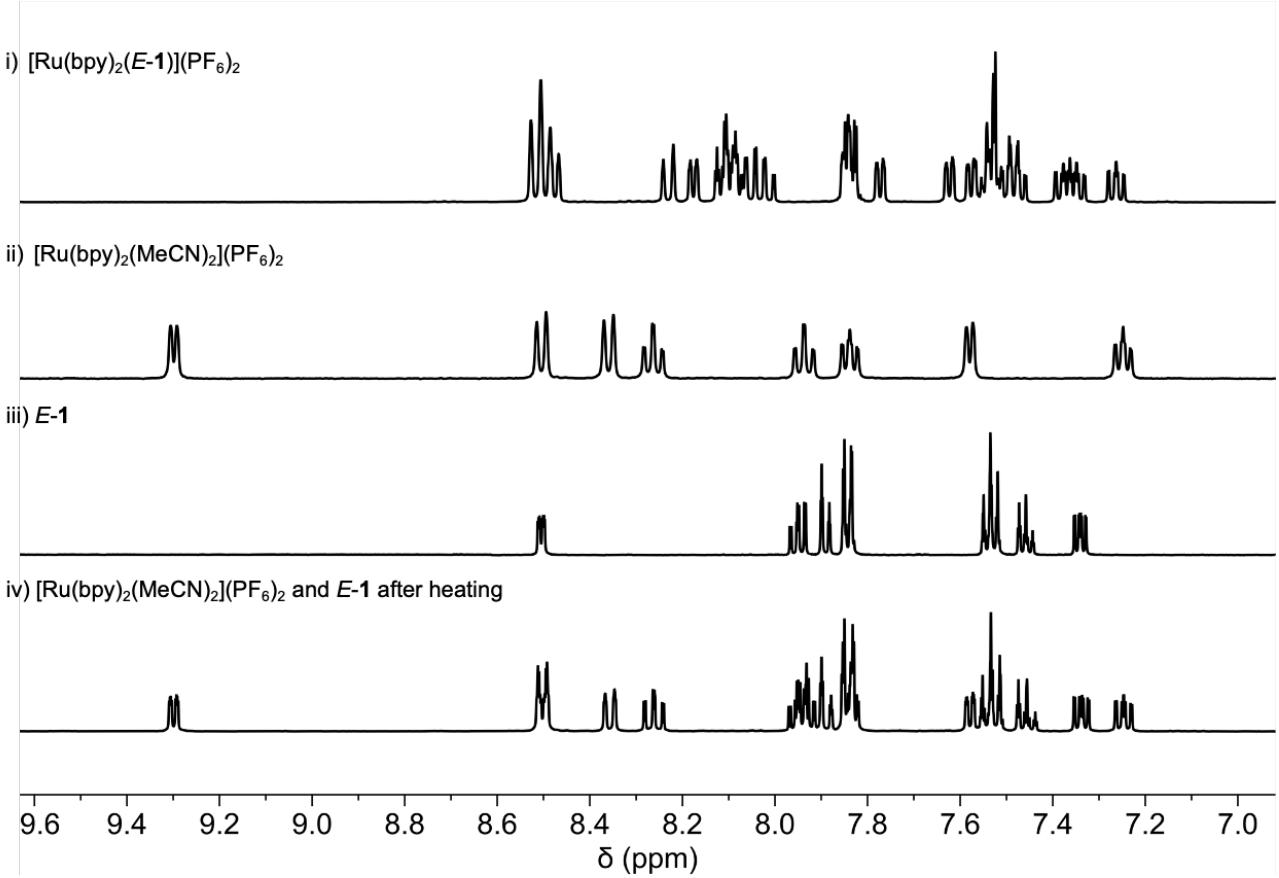

Figure S38. ^{1}H (500 MHz, 298 K, acetonitrile-d_3) NMR spectra of i) $[Ru(bpy)_2(E\text{-}\mathbf{1})](PF_6)_2$, ii) $[Ru(bpy)_2(MeCN)_2](PF_6)_2$, iii) ***E*-1**, iv) $[Ru(bpy)_2(MeCN)_2](PF_6)_2$ and *E*-**1** after heating for 1.75 hours at 50 °C.

S4.6 Diffusion NMR data for irradiated [Ru(bpy)$_2$(*E*-1)](PF$_6$)$_2$

The Bruker Avance III 400 MHz instrument with a Prodigy CryoProbe used the diff5 program with the Bruker diffSte pulsed-gradient stimulated echo (PGSTE) pulse sequence, with gradient length δ and echo delay Δ as specified in each experiment, including a spoiler gradient (followed by a 1.5 s recovery) to destroy magnetization remaining from the gradient pulse. Sine-shaped gradient pulses were used, typically ranging from 2-51 G cm^{-1}.

The gradient strength was calibrated using the known diffusion coefficient of the residual protons in D_2O at 298 K (1.93×10^{-9} m^2 s^{-1}).[10] The calibration was performed after data collection (prior to analysis) by correcting the nominal *b* values by the resulting calibration factor of 0.928.

Using the standard Stejskal–Tanner equation:[11]

$$I = I_0 \exp\left[-D\gamma^2 g^2 \delta^2 \left(\Delta - \frac{1}{3}\delta\right)\right] = I_0 \exp\left[-Db\right]$$

where I_0 is the NMR signal intensity in the absence of the applied gradient, γ is the gyromagnetic ratio of the nucleus, g and δ describe the amplitude and duration of the magnetic field gradient pulse, respectively, and the delay Δ defines the timescale over which diffusion is measured.

Estimates of the diffusion coefficient, D, and I_0 are determined by nonlinear regression of Stejskal–Tanner equation onto the signal integral data.

A sample of [Ru(bpy)$_2$(*E*-**1**)](PF$_6$)$_2$ in acetonitrile-d_3 was irradiated with 365 nm light for 3.5 hours and was measured using two experiments (Figure S39, Figure S40) each with a different δ and Δ value. An integral at 3.23 ppm corresponding to H^{B2} of [Ru(bpy)$_2$(*E*-**1**)](PF$_6$)$_2$ an integral of the unknown species at 2.85 ppm (Figure S33) was analysed to determine the diffusion coefficient (Table S6).

Table S6. δ and Δ values and diffusion coefficient of [Ru(bpy)$_2$(*E*-**1**)](PF$_6$)$_2$ and peak at 2.85 ppm.

Experiment Number	δ / ms	Δ / ms	*D* of H^{B2} of [Ru(bpy)$_2$(*E*-**1**)](PF$_6$)$_2$ / 10^{-9} m^{2}s^{-1}	*D* of peak at 2.85 ppm / 10^{-9} m^{2}s^{-1}
1	1.5	51.4	1.19	1.23
2	1.5	47.8	1.19	1.17
Average			1.19	1.20 ± 0.04

The diffusion coefficient for the signal of H^{B2} of [Ru(bpy)$_2$(*E*-**1**)](PF$_6$)$_2$ has the same diffusion coefficient as the peak at 2.85 ppm (Table S6). This implies that both [Ru(bpy)$_2$(*E*-**1**)](PF$_6$)$_2$ and the unknown species that forms under irradiation at 365 nm light is similar in size.

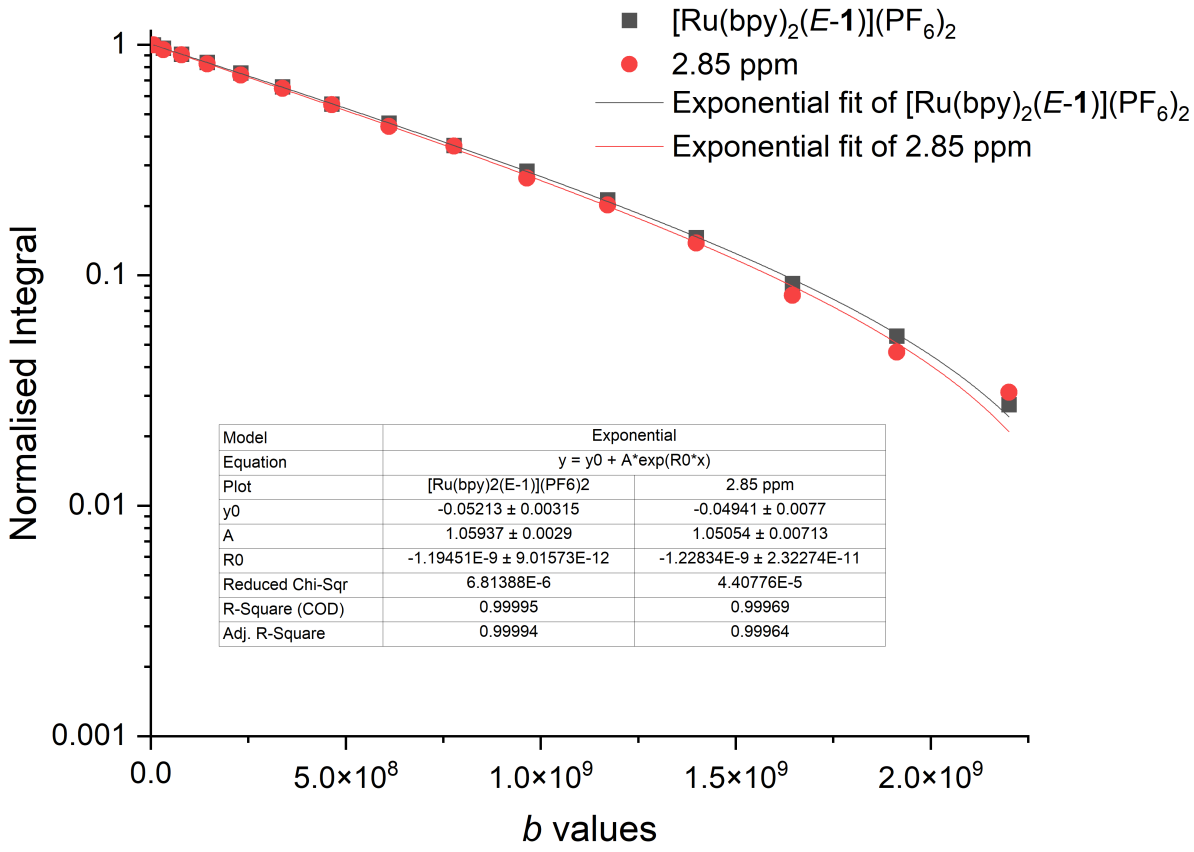

Model	Exponential	
Equation	y = y0 + A*exp(R0*x)	
Plot	[Ru(bpy)2(E-1)](PF6)2	2.85 ppm
y0	-0.05213 ± 0.00315	-0.04941 ± 0.0077
A	1.05937 ± 0.0029	1.05054 ± 0.00713
R0	-1.19451E-9 ± 9.01573E-12	-1.22834E-9 ± 2.32274E-11
Reduced Chi-Sqr	6.81388E-6	4.40776E-5
R-Square (COD)	0.99995	0.99969
Adj. R-Square	0.99994	0.99964

Figure S39. Diffusion NMR fitting for the signal of H^{B2} of [Ru(bpy)$_2$(*E*-**1**)](PF$_6$)$_2$ and signal at 2.85 ppm from ^{1}H NMR diffusion experiment: ste, δ = 1.5 ms, Δ = 51.4 ms. Data was fit to a monoexponential using corrected gradient values ($G_{corrected} = G_{app} \times 0.928$).

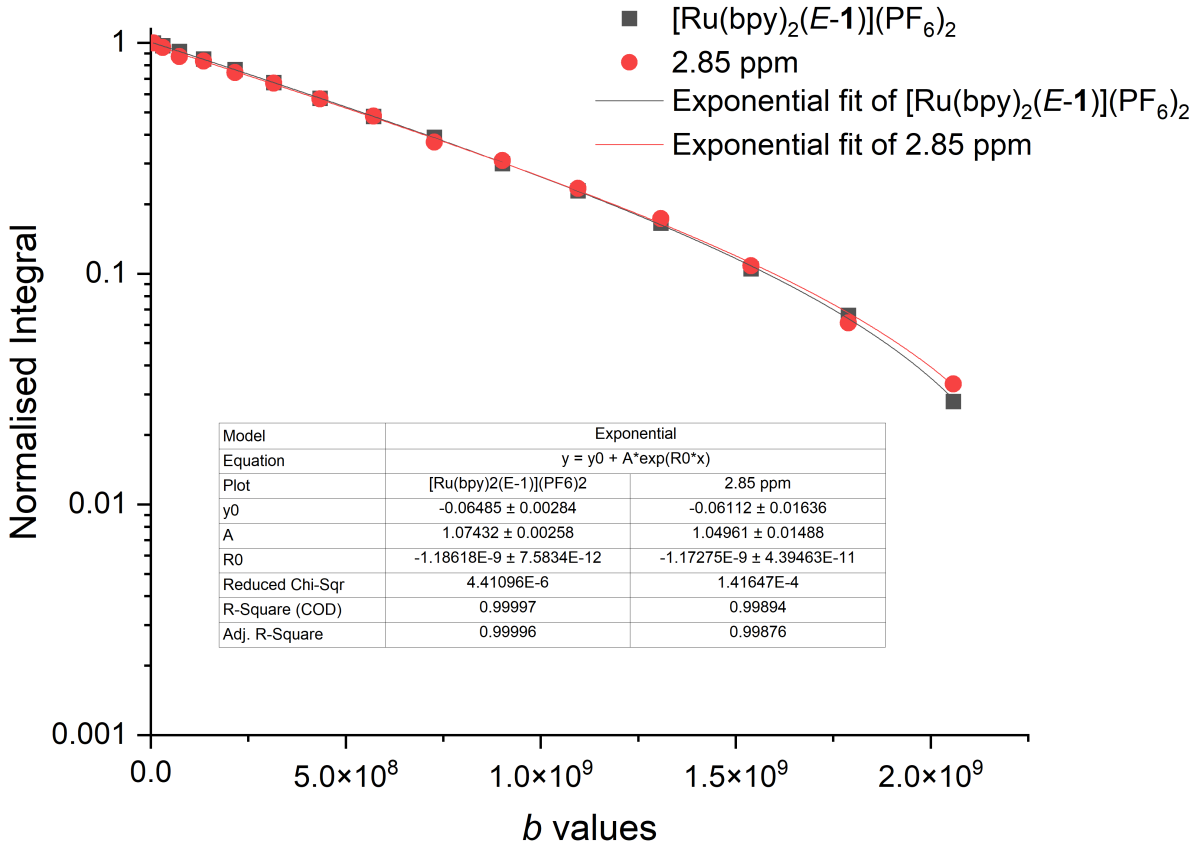

Model	Exponential	
Equation	y = y0 + A*exp(R0*x)	
Plot	[Ru(bpy)2(E-1)](PF6)2	2.85 ppm
y0	-0.06485 ± 0.00284	-0.06112 ± 0.01636
A	1.07432 ± 0.00258	1.04961 ± 0.01488
R0	-1.18618E-9 ± 7.5834E-12	-1.17275E-9 ± 4.39463E-11
Reduced Chi-Sqr	4.41096E-6	1.41647E-4
R-Square (COD)	0.99997	0.99894
Adj. R-Square	0.99996	0.99876

Figure S40. Diffusion NMR fitting for the signal of H^{B2} of [Ru(bpy)$_2$(*E*-**1**)](PF$_6$)$_2$ and signal at 2.85 ppm from ^{1}H NMR diffusion experiment: ste, δ = 1.5 ms, Δ = 47.8 ms. Data was fit to a monoexponential using corrected gradient values ($G_{corrected} = G_{app} \times 0.928$).

S5. Mass spectrometry analysis of species formed during irradiation

S5.1 Mass spectrometry analysis of [Ru(bpy)$_2$(*E*-1)](PF$_6$)$_2$

High-resolution electrospray ionization mass spectrometry (HR-ESI-MS) was collected in acetonitrile of [Ru(bpy)$_2$(*E*-**1**)](PF$_6$)$_2$ in the dark and after irradiation with a 365 nm light for 1 minute and 5 minutes (Figure S41). After 1 minute no new species were observed in the mass spectra. After 5 minutes peaks corresponding to [Ru(bpy)$_2$(MeCN)$_2$](PF$_6$)$_2$ and **1** are observed. No partially ejected complex, [Ru(bpy)$_2$(**1**)(MeCN)](PF$_6$)$_2$ was observed.

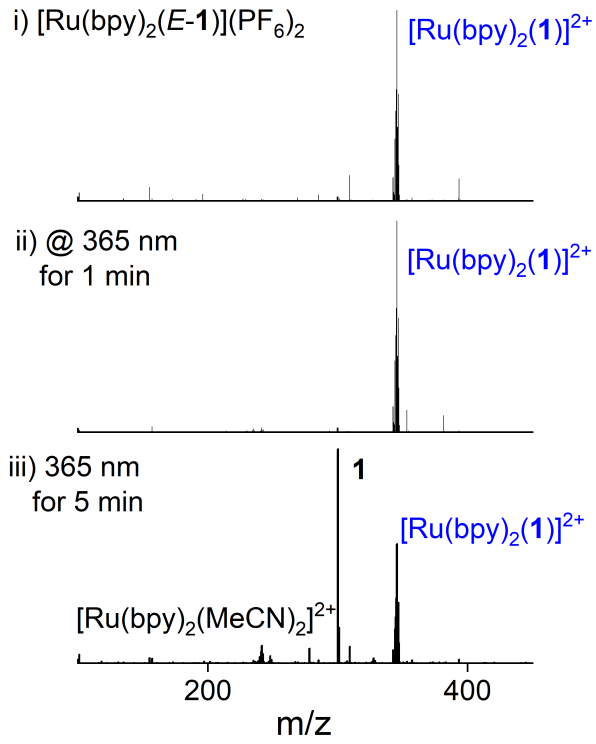

Figure S41. ESI-MS spectrum of [Ru(bpy)$_2$(*E*-**1**)](PF$_6$)$_2$ in acetonitrile i) in the dark, ii) after irradiation at 365 nm for 1 minute, and iii) after irradiation with 365 nm light for 5 minutes.

S5.2 Mass spectrometry analysis of $[Ru(bpy)_2(2)](PF_6)_2$

High-resolution electrospray ionization mass spectrometry (HR-ESI-MS) was collected in acetonitrile of $[Ru(bpy)_2(\mathbf{2})](PF_6)_2$ in the dark and after irradiation with a 365 nm light for 1 minute and 5 minutes (Figure S42). After 1 minute, peaks corresponding to $[Ru(bpy)_2(MeCN)_2](PF_6)_2$ and **2** was observed. No further changes were observed over 5 mins of irradiation. This contrasts with the behaviour of $[Ru(bpy)_2(\mathit{E}\text{-}\mathbf{1})](PF_6)_2$ where peaks corresponding to $[Ru(bpy)_2(MeCN)_2](PF_6)_2$ and the free ligand are only observed after 5 minutes.

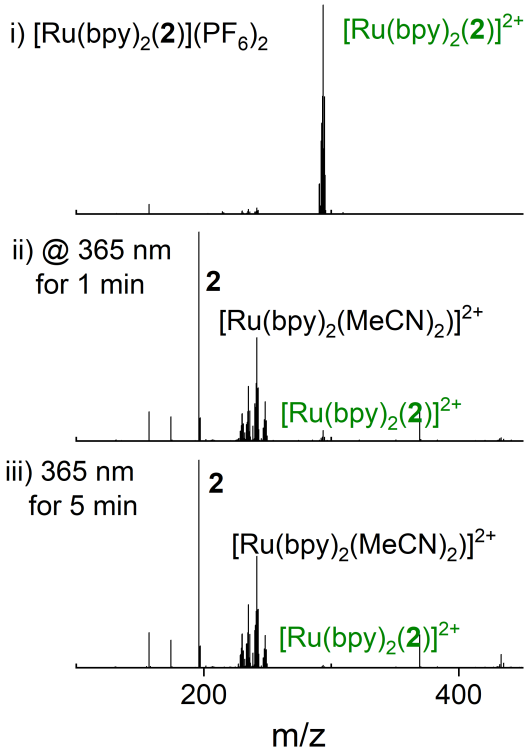

Figure S42. ESI-MS spectrum of $[Ru(bpy)_2(\mathbf{2})](PF_6)_2$ in MeCN i) in the dark, ii) after irradiation at 365 nm for 1 minute, and iii) after irradiation at 365 nm for 5 minutes.

S6. Single Crystal X-ray structural data

S6.1 Single crystal X-ray data of *E*-1 (CCDC: 2417092)

A needle-like single crystal with dimensions of 0.012 × 0.013 × 0.08 mm was selected under a polarizing microscope, and was mounted on a MicroMount, consisting of a thin polymer tip with a wicking aperture. X-ray diffraction data was collected at 100 K on the MX1[12] Macromolecular Crystallography beamline at the Australian Synchrotron at a wavelength of 0.71073 Å. The data collection and integration were performed within the AS QEGUI and XDS[13] software programs. The solutions were obtained by intrinsic phasing using SHELXT[14, 15] followed by successive refinements using full matrix least squares method against F2 using SHELXL-2018/3.[16, 17] The program OLEX2[18] was used was used as a graphical SHELX interface. All non-hydrogen atoms were refined with anisotropic thermal parameters, with hydrogen atoms being added geometrically and refined using riding thermal parameters. Due to the software set up at Australian Synchrotron, absorption correction and transmission factors are not reported.

Table S7. Crystal data and structure refinement for *E*-**1**

Crystallographic Details	*E*-**1**
Empirical formula	C16H15N5
Formula weight	277.33
Temperature/K	100(2)
Crystal system	monoclinic
Space group	P21/c
a/Å	16.220(3)
b/Å	4.6800(9)
c/Å	18.100(4)
α/°	90
β/°	94.20(3)
γ/°	90
Volume/Å3	1370.3(5)
Z	4
ρcalcg/cm3	1.344
μ/mm-1	0.085
F(000)	584.0
Crystal size/mm3	0.13 × 0.08 × 0.012
Radiation	Synchrotron (λ = 0.71073)
2Θ range for data collection/°	2.518 to 57.07
Index ranges	-21 ≤ h ≤ 21, -5 ≤ k ≤ 6, -24 ≤ l ≤ 23
Reflections collected	31207
Independent reflections	3124 [Rint = 0.0379, Rsigma = 0.0198]
Data/restraints/parameters	3124/0/192
Goodness-of-fit on F2	1.105
Final R indexes [I>=2σ (I)]	R1 = 0.0631, wR2 = 0.2003
Final R indexes [all data]	R1 = 0.0802, wR2 = 0.2294
Largest diff. peak/hole / e Å-3	0.48/-0.48

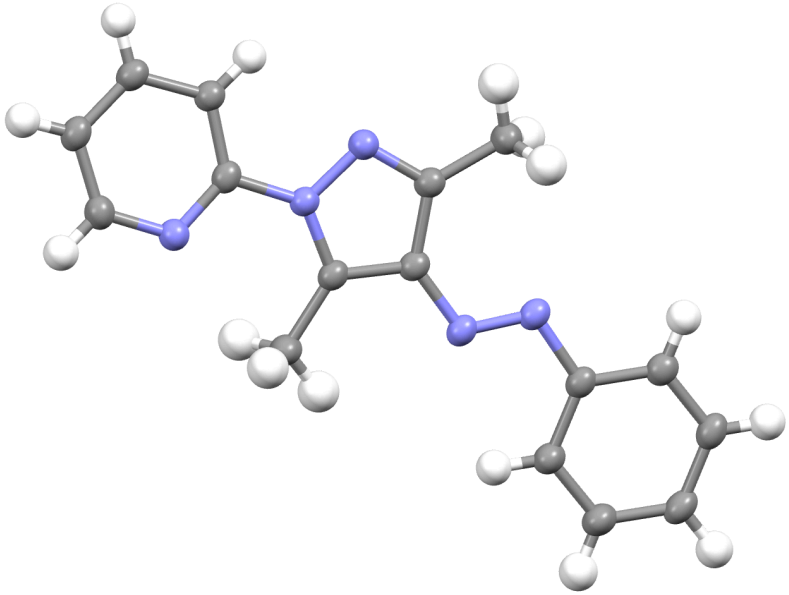

Figure S43. ORTEP representation of *E*-**1**. Ellipsoids are drawn at 50% probability.

S6.2 Single crystal X-ray data of $[Ru(bpy)_2(E\text{-}1)](PF_6)_2$ (CCDC: 2417124)

Crystals suitable for X-ray crystallography were grown by the slow evaporation of diethyl ether into a solution of $[Ru(bpy)_2(\mathbf{1})](PF_6)_2$ in acetonitrile. A block-like single crystal with dimensions of 0.062 × 0.095 × 0.31 mm was selected under a polarizing microscope (Leica M165Z), and was mounted on a MicroMount (MiTeGen, USA), consisting of a thin polymer tip with a wicking aperture. The X-ray diffraction measurements were carried out on a Bruker D8 Quest Single Crystal diffractometer with a Photon II detector at 120 K by using μS 3.0 Microfocus Source with Mo-Kα radiation (λ = 0.710723 Å). The single crystal was coated with NVH immersion oil and then quickly transferred to the cold nitrogen stream using the Oxford Cryostream 800 series attachment, and it was mounted on the goniometer using a cryo loop for intensity measurement. The solutions were obtained by intrinsic phasing using SHELXT[14, 15] followed by successive refinements using full matrix least squares method against F2 using SHELXL-2018/3.[16, 17] The program OLEX2[18] was used was used as a graphical SHELX interface. All non-hydrogen atoms were refined with anisotropic thermal parameters, with hydrogen atoms being added geometrically and refined using riding thermal parameters.

Table S8. Crystal data and structure refinement for $[Ru(bpy)_2(E\text{-}\mathbf{1})](PF_6)_2$

Crystallographic Details	$[Ru(bpy)_2(E\text{-}\mathbf{1})](PF_6)_2$
Empirical formula	C40H42F12N9OP2Ru
Formula weight	1055.83
Temperature/K	101.00
Crystal system	monoclinic
Space group	P21
a/Å	12.8968(7)
b/Å	12.6940(6)
c/Å	12.9165(7)
α/°	90
β/°	91.706(2)
γ/°	90
Volume/Å3	2113.65(19)
Z	2
ρcalcg/cm3	1.659
μ/mm-1	0.546
F(000)	1070.0
Crystal size/mm3	0.308 × 0.095 × 0.062
Radiation	MoKα (λ = 0.71073)
2Θ range for data collection/°	4.5 to 46.598
Index ranges	-14 ≤ h ≤ 14, -14 ≤ k ≤ 14, -14 ≤ l ≤ 14
Reflections collected	55588
Independent reflections	6079 [Rint = 0.1025, Rsigma = 0.0489]
Data/restraints/parameters	6079/43/531
Goodness-of-fit on F2	1.146
Final R indexes [I>=2σ (I)]	R1 = 0.0596, wR2 = 0.1423
Final R indexes [all data]	R1 = 0.0824, wR2 = 0.1702
Largest diff. peak/hole / e Å-3	1.52/-1.05
Flack parameter	-0.01(2)

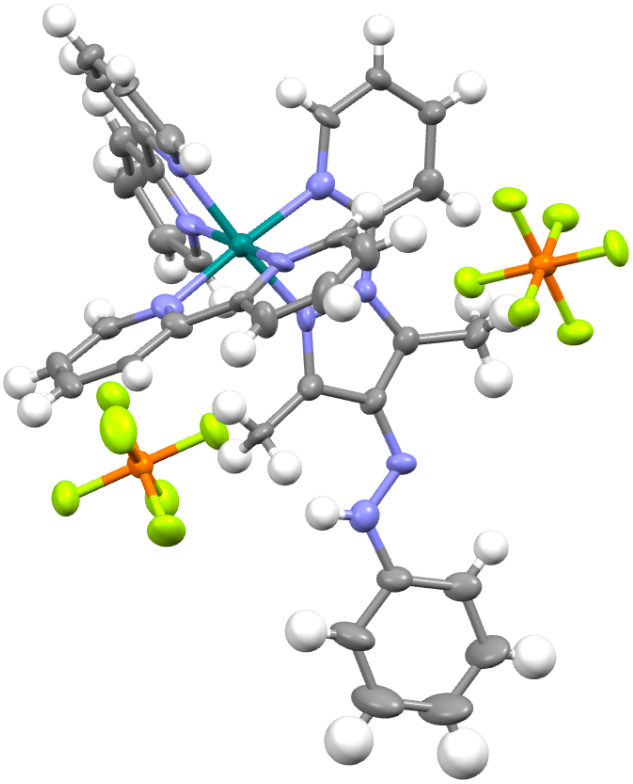

Figure S44. ORTEP representation of [Ru(bpy)$_2$(*E*-**1**)](PF$_6$)$_2$. Ellipsoids are drawn at 50% probability.

S6.3 Single crystal X-ray data of $[Ru(bpy)_2(2)](PF_6)_2$ (CCDC: 2417094)

Crystals suitable for X-ray crystallography were grown by the slow evaporation of diethyl ether into a solution of $[Ru(bpy)_2(\mathbf{2})](PF_6)_2$ in acetonitrile. A block-like single crystal with dimensions of 0.062 × 0.095 × 0.31 mm was selected under a polarizing microscope (Leica M165Z), and was mounted on a MicroMount (MiTeGen, USA), consisting of a thin polymer tip with a wicking aperture. The X-ray diffraction measurements were carried out on a Bruker D8 Quest Single Crystal diffractometer with a Photon II detector at 120 K by using μS 3.0 Microfocus Source with Mo-Kα radiation (λ = 0.710723 Å). The single crystal was coated with NVH immersion oil and then quickly transferred to the cold nitrogen stream using the Oxford Cryostream 800 series attachment, and it was mounted on the goniometer using a cryo loop for intensity measurement. The solutions were obtained by intrinsic phasing using SHELXT[14, 15] followed by successive refinements using full matrix least squares method against F2 using SHELXL-2018/3.[16, 17] The program OLEX2[18] was used was used as a graphical SHELX interface. All non-hydrogen atoms were refined with anisotropic thermal parameters, with hydrogen atoms being added geometrically and refined using riding thermal parameters.

The structure showed that ligand **2** is equally disordered over all three ligand positions.

Table S9. Crystal data and structure refinement for $[Ru(bpy)_2(\mathbf{2})](PF_6)_2$.

Crystallographic Details	$[Ru(bpy)_2(\mathbf{2})](PF_6)_2$
Empirical formula	C30H24F12N6P2Ru
Formula weight	859.56
Temperature/K	120.15
Crystal system	trigonal
Space group	P-3c1
a/Å	10.6119(5)
b/Å	10.6119(5)
c/Å	16.8356(8)
α/°	90
β/°	90
γ/°	120
Volume/Å3	1641.90(17)
Z	2
ρcalcg/cm3	1.739
μ/mm-1	0.677
F(000)	856.0
Crystal size/mm3	? × ? × ?
Radiation	MoKα (λ = 0.71073)
2Θ range for data collection/°	4.432 to 55.1
Index ranges	-13 ≤ h ≤ 13, -13 ≤ k ≤ 13, -21 ≤ l ≤ 21
Reflections collected	66682
Independent reflections	1260 [Rint = 0.0610, Rsigma = 0.0127]
Data/restraints/parameters	1260/0/79
Goodness-of-fit on F2	1.041
Final R indexes [I>=2σ (I)]	R1 = 0.0725, wR2 = 0.1857
Final R indexes [all data]	R1 = 0.0886, wR2 = 0.2146
Largest diff. peak/hole / e Å-3	1.15/-0.90

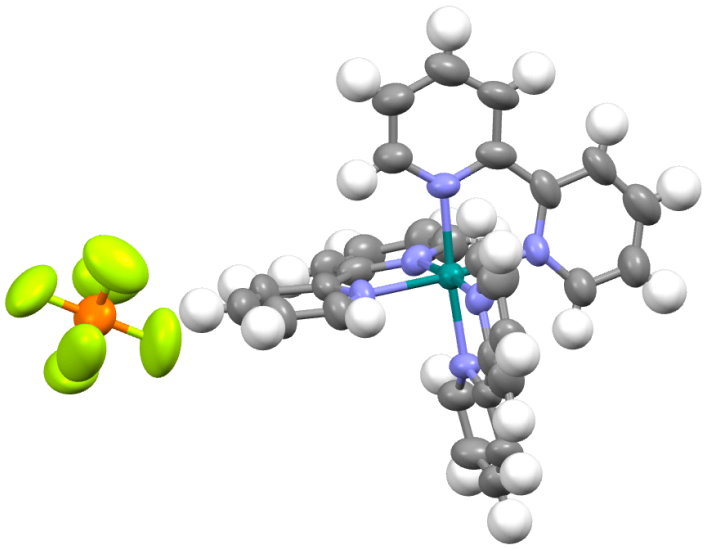

Figure S45. ORTEP representation of [Ru(bpy)$_2$(**2**)](PF$_6$)$_2$. Ellipsoids are drawn at 50% probability.

S7. References

1. C. E. Weston, R. D. Richardson, P. R. Haycock, A. J. P. White and M. J. Fuchter, *J. Am. Chem. Soc.*, 2014, **136**, 11878-11881.
2. D. Gupta, A. K. Gaur, R. Kaur, Ashish, N. Kaur and S. Venkataramani, *Chem.– Eur. J.*, 2023, **29**, e202301906.
3. Y. Takahira, E. Murotani, K. Fukuda, V. Vohra and H. Murata, *J. Fluorine Chem.*, 2016, **181**, 56-60.
4. E. T. Luis, G. E. Ball, A. Gilbert, H. Iranmanesh, C. W. Newdick and J. E. Beves, *J. Coord. Chem.*, 2016, **69**, 1686-1694.
5. B. P. Sullivan, D. J. Salmon and T. J. Meyer, *Inorg. Chem.*, 1978, **17**, 3334-3341.
6. A.-C. Laemmel, J.-P. Collin and J.-P. Sauvage, *Eur. J. Inorg. Chem.*, 1999, **1999**, 383-386.
7. P. J. Steel, F. LaHousse, D. Lerner and C. Marzin, *Inorg. Chem.*, 1983, **22**, 1488-1493.
8. G. M. Brown, R. W. Callahan and T. J. Meyer, *Inorg. Chem.*, 1975, **14**, 1915-1921.
9. T. L. Rapp, S. R. Phillips and I. J. Dmochowski, *Journal of Chemical Education*, 2016, **93**, 2101-2105.
10. W. S. Price, *NMR Studies of Translational Motion: Principles and Applications*, Cambridge University Press, Cambridge, 2009.
11. E. O. Stejskal and J. E. Tanner, *J. Chem. Phys.*, 1965, **42**, 288-292.
12. T. M. McPhillips, S. E. McPhillips, H. J. Chiu, A. E. Cohen, A. M. Deacon, P. J. Ellis, E. Garman, A. Gonzalez, N. K. Sauter, R. P. Phizackerley, S. M. Soltis and P. Kuhn, *J. Synchrotron Rad.*, 2002, **9**, 401-406.
13. W. Kabsch, *Acta Crystallogr D Biol Crystallogr*, 2010, **66**, 125-132.
14. G. M. Sheldrick, *Acta Cryst. A*, 2008, **64**, 112-122.
15. G. M. Sheldrick, *Acta Crystallogr A*, 2008, **64**, 112-122.
16. G. M. Sheldrick, *Acta Crystallographica Section C: Structural Chemistry*, 2015, **71**, 3-8.
17. G. M. Sheldrick, *Acta Crystallogr C Struct Chem*, 2015, **71**, 3-8.
18. O. V. Dolomanov, L. J. Bourhis, R. J. Gildea, J. A. K. Howard and H. Puschmann, *J. Appl. Crystallogr.*, 2009, **42**, 339-341.